Department of Electrical and Computer Systems Engineering

Technical Report MECSE-9-2004

Advanced Sonar Ring Sensing in Theory and Practice

S. Fazli, L. Kleeman

Advanced Sonar Ring Sensing in Theory and Practice

Saeid Fazli and Lindsay Kleeman
(Saeid.fazli | Lindsay.kleeman)@eng.monash.edu.au

ARC Centre for Perceptive and Intelligent Machines in Complex Environments (PIMCE)
Intelligent Robotics Research Centre (IRRC)
Monash University, Australia

Abstract

Conventional sonar ring sensors, which can measure the distance to the nearest objects, are widely used in indoor mobile robots for obstacle avoidance purposes. Meanwhile, in advanced sonar sensing, accurate range and bearing measurement of multiple targets is performed using multiple receivers in each direction, but often regarded as slow due to the intensive computation process of all captured echoes, therefore it is difficult to perform on-the-fly applications such as map building, target tracking and localization using a conventional sonar ring due to low speed, accuracy and also interference. This report presents an *advanced sonar ring* that employs a low receiver sample rate to achieve processing of 48 receiver channels at near real time repetition rates of 15 Hz. The sonar ring sensing covers 360 degrees around the robot, depending on the environment, for ranges up to six metres, with simultaneously firing of 24 transmitters. Digital Signal Processing (DSP) techniques and interference rejection ideas are applied in this sensor to design a new more sophisticated, fast and accurate sonar ring. The advanced sonar ring consists of 48 ultrasonic transducers 24 acting as transceivers and 24 acting as receivers, seven DSP echo processor boards, twelve four-channel 12-bit multiplexed 500 kHz ADCs and low noise variable gain preamplifiers. The receiver sampling frequency is 250 kHz, compared to previous work at 1 MHz, firstly to maximize the speed of processing and secondly to avoid memory limitations of the DSPs. The processing to produce accurate distance and bearing measurements is performed on 6 DSPs using template matching of echoes with short duration. This report presents a summary of the hardware architecture, software architecture and sensing theory of the *advanced sonar ring*. The use of a reference point and offset table is introduced and experimentally verified to improve the sensor accuracy and robustness. The problem and solution to cycle hopping, caused by the low sampling rate, are described in the report. Also the report presents new transmit coding based on pulse duration to differentiate neighbouring transmitters in the ring. Experimental data show the effectiveness of the designed sensor.

1. Introduction

Sonar ring sensors provide robots with low cost accurate range finders. A sonar ring is a set of sonar sensors configured around the robot to provide sensing of the surrounding environment without the mechanical complication and delays associated with scanning sensors. Conventional sonar rings deploy Polaroid ranging modules or equivalent and suffer from poor bearing accuracy and interference problems [4,15]. Furthermore, a fast, accurate and robust environment sensor is always a critical part of robotic tasks such as map building, localization, target tracking and collision avoidance. As an active sensor, sonar has advantages in accuracy, robustness and simplicity when compared with passive methods, such as vision or passive infra red. However, active sensing, and hence sonar, is subject to inter-sensor interference, requiring filtering to prevent erroneous measurements. Research in the past twenty years has progressively refined sonar's accuracy and increased its functionality. Accurate range and bearing measurements of multiple objects have been achieved [9-11,14], enabling sonar systems to produce accurate maps and to localize the sonar within them. Researchers have developed a sonar ring that allows simultaneous firing and thresholding of echo signals to measure reflectors with a bearing accuracy of around 1 degree [20,21]. Interference can be rejected [3,9,10], making possible the operation of multiple sonars in the same acoustic space, or in noisy spaces. This is important for cooperative robotics, swarm robotics or any time two sonar equipped mobile robots need to pass near each other. Meanwhile, Digital Signal Processor (DSP) systems have enabled the ultrasonic echo to be sampled at 12 bit amplitude resolution and 1 microsecond sample time and then processed in near real time to measure range to 0.2 mm and bearing to 0.1 degrees [8]. This approach is fast and accurate but operates in just one direction within the beamwidth of the transducers. Mechanical scanning and many measurements taken in sequence are needed to cover a full 360 degrees. With the decreasing cost and increasing performance of DSPs, it is now possible to perform intensive sonar echo processing around an entire ring of transducers from a single simultaneous set of transmissions in near real time. Thus the sequential scanning of the individual sonar sensors has been condensed into one measurement cycle of the advanced sonar ring. The use of DSP local processing relieves communication problems with a host computer as in [10] where all echo samples are sent through the computer bus. A second advantage is that the DSP offers optimised instructions for high-speed signal processing over a general purpose computer – in particular the matched filter operations are extremely fast. Thirdly, there is little signal degradation since the physical distance between receiver and pre-amplifiers is reduced, allowing much better shielding to the front end of the receiver electronics.

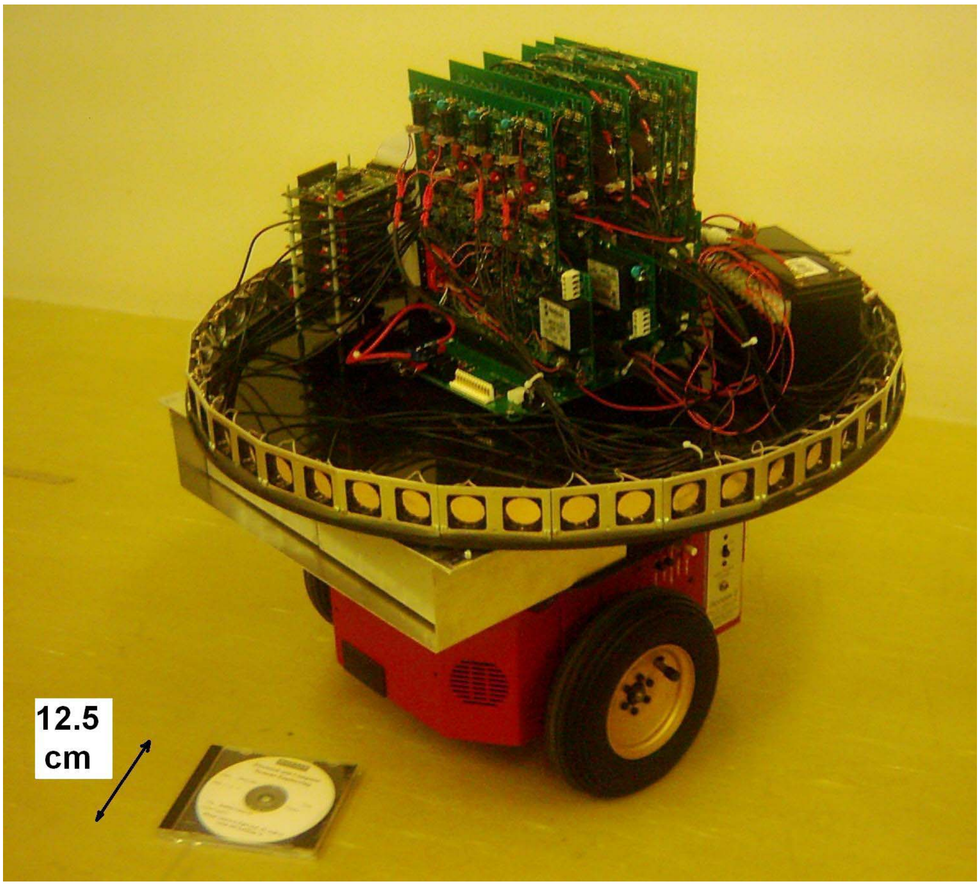

Figure 1. Advanced sonar ring mounted on an ActivMedia Pioneer 3 DX mobile robot.

This report presents the first self-contained sonar ring that achieves accurate and robust distance and range measurements around robot at near real time rates – termed an advanced sonar ring. The repetition rate of the sonar ring is limited by the time of flight to the furthest range of about 6 metres combined in parallel with DSP computation and serial communication between DSPs and a host computer. We achieve a repetition of approximately 15 Hz in this report. This report is partly based on a paper which has been accepted for publication at IROS 2004 [7] and a paper submitted to ACRA 2004 [6].

The sensor works by simultaneously firing of all transmitters and hence emitting a burst of ultrasound in all directions, and waiting the echoes reflected from any objects within the sound beam. The measured delay, known as the time-of-flight (TOF), of the returned echoes is proportional to the distance to the object. Then the bearing is determined by combining multiple measurements. The basic idea is to calculate TOF for each receiver by means of signal processing technique similar to that used in RADAR [18]. This technique is matched filtering (also called template matching) which is the minimum variance arrival time estimator in the presence of additive white Gaussian noise on the echo. A matched filter is based on finding the peak of the cross correlation of the echo with an *a priori* calculated template. This technique has been extensively used in [5,8,10,11]. This report presents a DSP sonar ring consisting of 48 transducers in 24 pairs each pair has a transceiver and a receiver so the ring has 24 transmitters firing simultaneously and 48 receivers. The simultaneous firing of a sonar ring has recently been used by other researchers for obstacle detection [16,17]. In the advanced sonar ring, the bearing calculation is based on the difference between arrival time of echo in two receivers and a triangulation technique. As each pair approximately 15 degrees, the sonar ring gets information from almost all of the full 360 degrees around robot. Each group of eight transducers is controlled by a local slave DSP that communicates with a single master DSP that in turn relays results of all slaves to a host computer over a serial line. One of the advantages of this configuration is that it relieves the computational burden of the host computer allowing computationally intensive applications to take place on a moving platform.

The next section briefly introduces hardware components of the advanced sonar ring. The sensing theory, known as matched filtering, is presented in section 3. This section shows that the maximum likelihood estimator of the arrival time of the echo corrupted by additive white Gaussian noise is the best estimator [13]. This theory is important for understanding and solving the problem of cycle hopping, discussed later.

Section 4 introduces the advanced sonar ring software architecture and the implementation of on-the-fly processing using highly optimised assembly code. This section also explains the implementation of matched filtering within a DSP context, yielding very accurate range and bearing estimation. Experimental results are presented in section 5 to show the effectiveness of the proposed system. In this section, also the concepts of reference point, offset table, cycle hopping rejection and interference rejection are explained. Conclusions and a discussion of further work are presented in the last section.

2. The Advanced Sonar Ring Hardware Architecture

The custom designed multi DSP sonar ring sensor is shown in Fig. 1 mounted on an ActivMedia Pioneer 3 DX mobile robot. The various components of the advanced sonar ring are described below.

2.1. A Ring Consisting of 48 Transducers

A group of eight Polaroid 7000 series transducers, arranged in four pairs, is controlled by a digital slave DSP board and an associated analogue board. The ring contains 24 pairs with each pair containing a transceiver and a receiver 40.5 mm and 15 degrees apart. The sensor is capable of covering full 360 degrees around robot when the effective beamwidth of each pair of transducers is at least 15 degrees and this occurs for highly reflective specular targets at ranges closer than 2.8 m. Fig. 2 shows the viewing area for a pair of transducers observing a plane target at positions out to 4 m range.

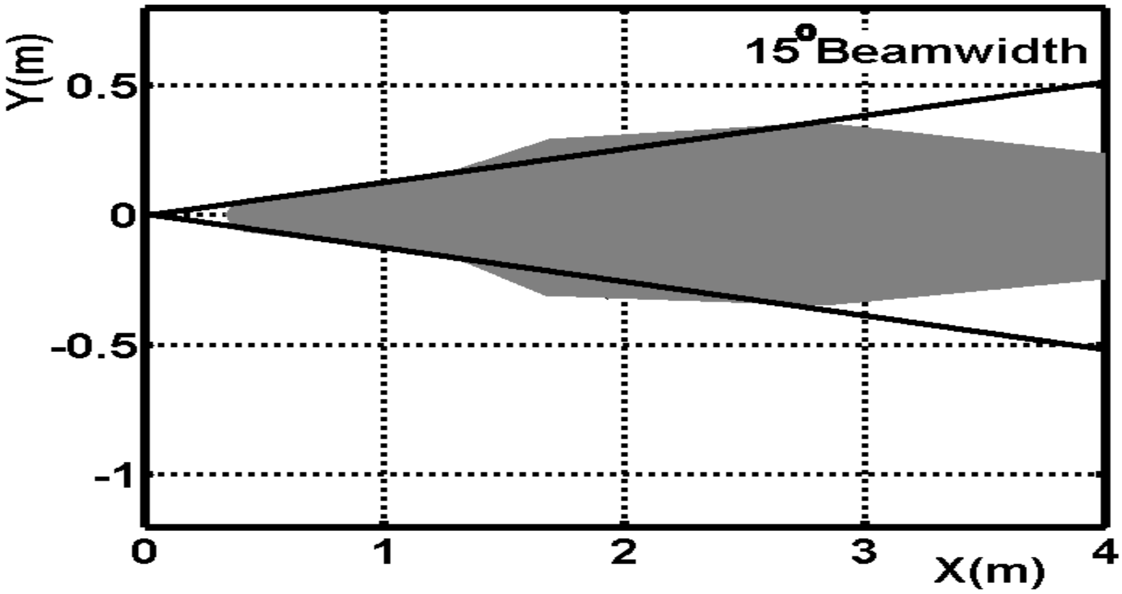

Figure 2. The measured beamwidth of a pair of transducers in gray – the solid line indicates the requirement for the ring to cover 360 degrees.

2.2. Six Analogue Slave PCBs

Each slave board is responsible for controlling the transmission and data acquisition process for four pairs of transceiver and receivers, grouped into four pairs. Also the board contains a high voltage DC-DC converter to produce a 300 V bias on the 8 transducers (Fig. 3).

2.3. Six Digital Slave PCBs

Each of the six digital slave boards contains a DSP and two Analog to Digital Converters (ADC) and connects to an analogue slave board via a ribbon cable (Fig. 4). The DSP is responsible for generating the transmit pulses for the four transceivers and processing the echoes collected by the eight transducers. Two 12-bit ADS7862 ADCs are configured to allow pairwise synchronised sampling of 8 input channels at 250 kHz sample rate. An Analog Devices 2189M DSP was chosen due to the single clock cycle access to on-chip RAM of 192 k bytes, allowing echoes to be extracted, stored and processed within the DSP chip. The speed of the on-chip memory allows the processor to fetch two operands (one from data memory and one from program memory) and an instruction (from program memory) in a single cycle.

2.4. A master PCB

A master board contains a 2189M DSP, flash memory and a high speed buffered UART (Fig. 5). It communicates with a central computer via the high speed serial link and with all the digital slave boards via a PC104 type connector using the Internal Direct Memory Access (IDMA) feature of the 2189M DSPs. The DSPs contain two DMA ports, Internal DMA port and Byte DMA port. The IDMA port provides an efficient means of access the on-chip program memory and data memory of the DSP with only one cycle per word of overhead. The IDMA port has a 16-bit multiplexed address and data bus and supports 24-bit program memory. The IDMA port is completely asynchronous and can be written to while the ADSP 2189M is operating at full speed [2].

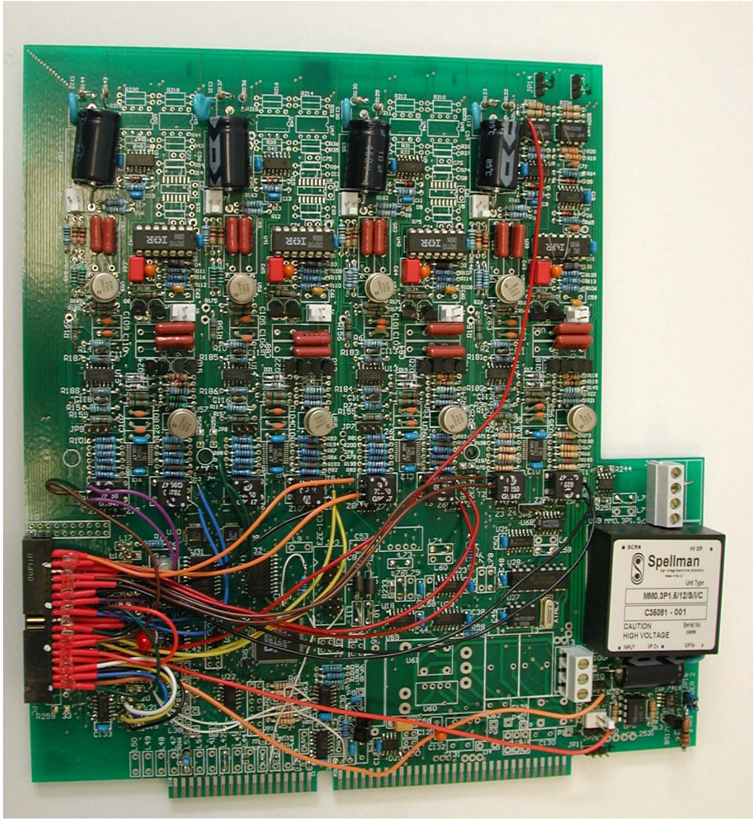

Figure 3. An Analogue Slave PCB.

In the first design, the advanced sonar ring contained both analogue slave and digital slave on the same PCB but due to the high speed of the IDMA between slave processors and master processor communication errors were encountered. The digital part was re-designed on a four layer board and the analogue slave was separated. In addition, we have encountered problems protecting the ADCs from being destroyed through power supply transients and electrostatic discharge during construction.

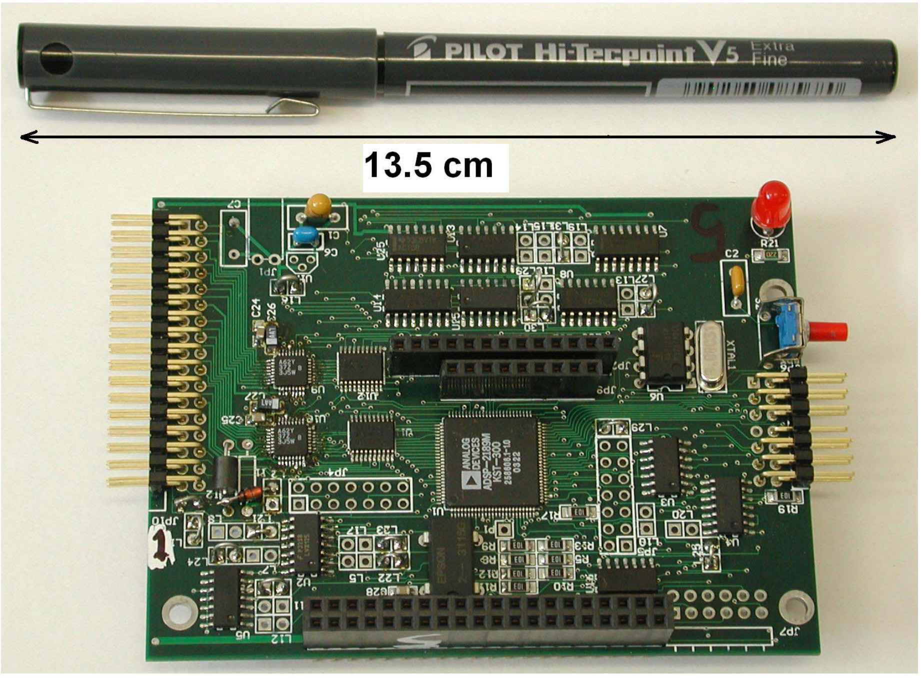

Figure 4. A Digital Slave PCB.

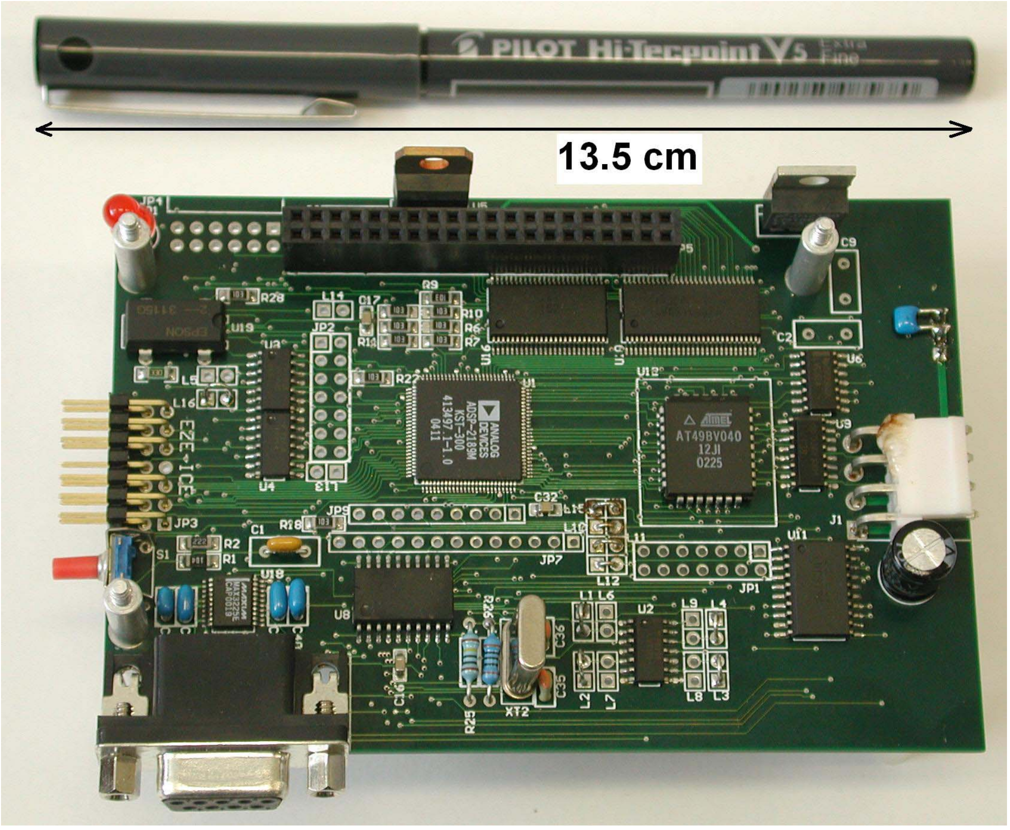

Figure 5. A Master PCB.

Fig. 6 shows the block diagram of the hardware architecture. The receiver channels are amplified and low pass filtered before sampling with ADCs at 250 kHz. The transmitter circuitry allows a programmable digital pulse train to be sent to the transducer without the need for preloaded memory buffers as required previously [10]. Instead the slave DSP directly controls the transmit logic every microsecond under interrupt control. Varying gain preamplifiers increase the gain in a fixed profile after each firing. The master board sends all commands and reads the high level data from slave boards via a PC104 type connector, using IDMA of the DSP which allows high speed access to on-chip memory of the slave DSPs. The master DSP relays results from all slaves to a host computer using a RS232 serial port.

3. The Advanced Sonar Ring Sensing Theory

The operation of the advanced sonar ring relies solely on Time-Of-Flight (TOF) information. The TOF is a measure of when received pulse is detected, relative to the time the pulse was transmitted. The performance of this sonar ring in localizing targets depends heavily on the accurate estimation of the TOF. In conventional sonar systems, a return pulse is detected at a receiver if the received signal exceeds a predetermined threshold. The TOF is the time at which the received signal surpasses the threshold. This method of estimating the TOF is susceptible to noise in the received signal and does not account for the changes in the sonar pulse shape. Consequently, the accuracy of this technique is limited while in reality the accuracy achievable with sonar can be far better [1]. This justifies the use of a more sophisticated method to achieve better accuracy in TOF estimation.

A matched filter is obtained by examining the cross correlation of the echo containing noise with the predicted pulse shape. The arrival time corresponds to the time shifted position of the predicted pulse that gives a maximum in the cross correlation [11,12]. Theory of Radar shows that the Maximum Likelihood Estimator of the arrival time of the echo corrupted by additive white Gaussian noise is the matched filter [13]. This means that it is usually the best estimator in practice. The problem with the matched filter is predicting the echo pulse shape, since it depends on the bearing angle to the target, dispersion in air of ultrasound, scattering properties of targets and transmitter and receiver characteristics. Linear models exist that accurately predict pulse shape and matched filtering has been implemented successfully [12].

3.1. Theory of Radar Reception

The basic idea of radar reception is to calculate the delay of an echo from a received noisy signal. In this section we show that the matched filtering is the best arrival time estimator in theory. Equations (1-6) are based on [13] and justify the optimality of the arrival time estimation used in the advanced sonar ring.

The problem is to extract the information from a noisy received signal. We assume that the wanted information in the receiver is x, noise is white Gaussian and the received signal is denoted by y. The signal y is available and we require the probability distribution $p\ (x \mid y)$, which gives us some information about x from the knowledge of y.

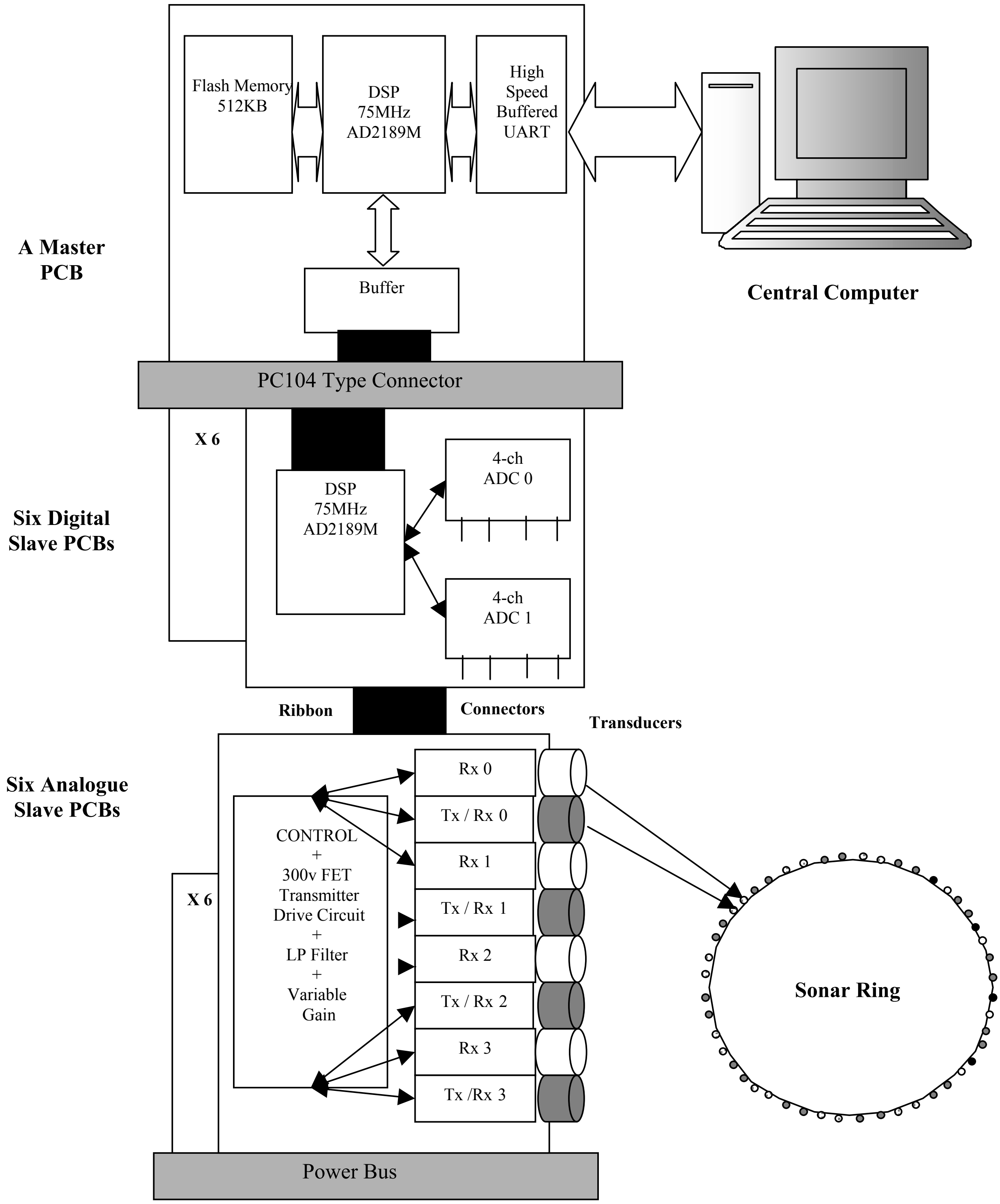

Figure 6. Advanced sonar ring hardware block diagram

The calculation of $p\ (x\,|\,y)$ is a problem of inverse probability. The product law for probabilities is

$$p(x,y) = p(x)p(y\,|\,x) = p(y)p(x\,|\,y) \tag{1}$$

and since y is given, the second side of these equations may be written

$$p\ (x\,|\,y) = k\ \ p(x)p\ (y\,|\,x) \tag{2}$$

where k is the normalizing constant of distribution. In equation (2) $p(x)$ is the prior probability of x and $p\ (x\,|\,y)$ is the posterior probability of x .

If we denote u_x as a time-dependent signal representing the information x and n as additive white Gaussian noise, then the received waveform is

$$y = u_x + n \tag{3}$$

which is available in the receiver and the reception method should determine $p\ (x \mid y)$.

The Likelihood Function is written as

$$p\ (y \mid x) = k\exp(-E/N_0) = k\exp\{-\frac{1}{N_0}\int (y-u_x)^2 dt\} \tag{4}$$

where N_0 is N/W, N is the mean noise power and W is the bandwidth of the signal. The integral in the equation is definite and the limits must correspond to the total interval of time occupied by the signal. The term y^2 can be absorbed into k

$$p\ (x \mid y) = k\quad p(x)\exp\{-\frac{1}{N_0}\int {u_x}^2 dt\}\exp\{\frac{2}{N_0}\int y u_x dt\} \tag{5}$$

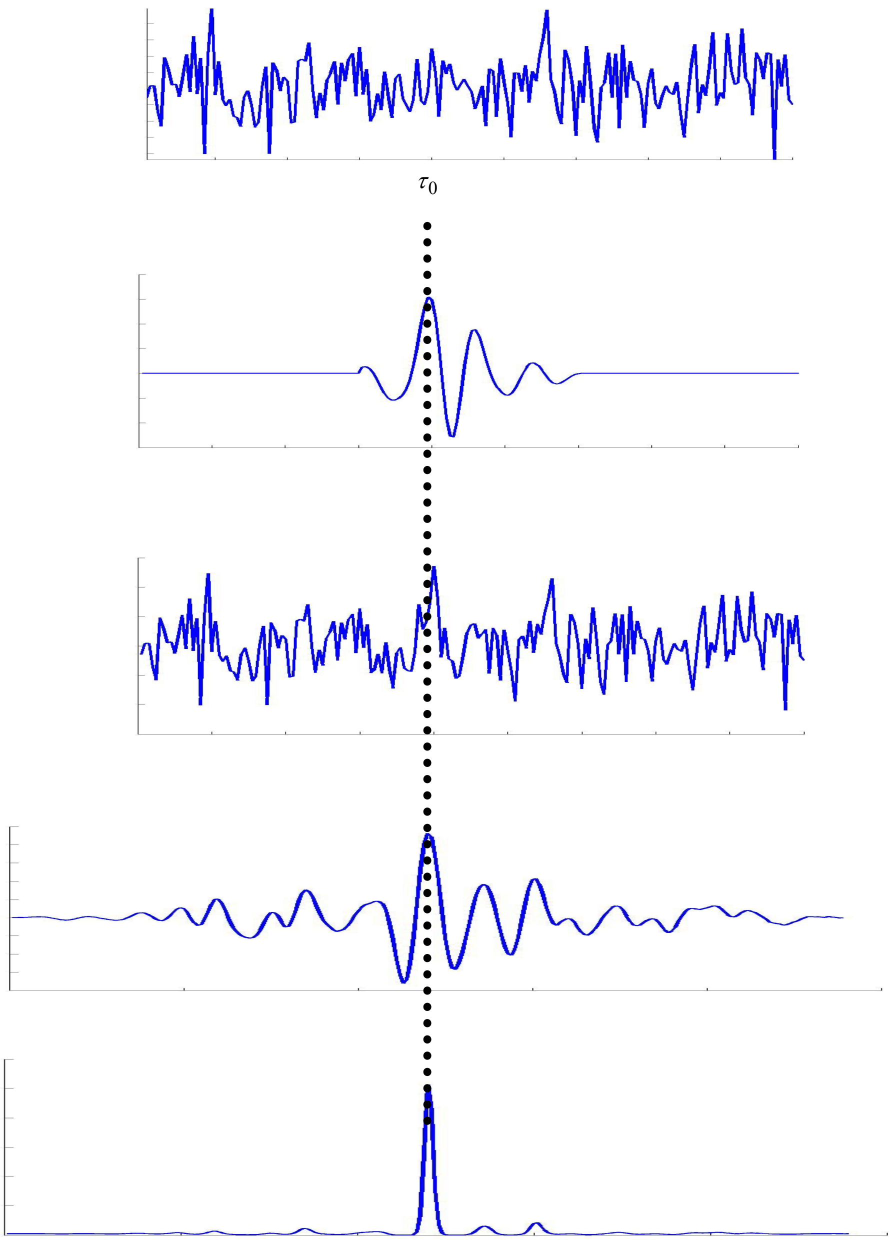

Figure 7. (a) Gaussian noise, (b) signal at t= τ_0 , (c) noise + signal, (d) $q(\tau)$, (e) posterior distribution for τ (Note: The length of the signals d and e are bigger than a,b and c due to the croos correlation)

Equation (5) shows that the term

$$q(x) = \int y u_x dt \tag{6}$$

is the only term that depends on y and using that we can obtain all information about posterior distribution. Equation (6) is a cross correlation between the received signal, y and a predicted noiseless received signal, u_x.

In discrete form, equation (5) becomes:

$$p\ (x \mid y) = kp(x)\exp\{-\frac{1}{N_0}\sum_t {u_x}^2\}\exp\{\frac{2}{N_0}\sum_t y u_x\} \tag{7}$$

Now let us continue with the problem of range finding or TOF estimation. The pulse shape will be denoted by $u(t)$, a delay of τ occurs in the pulse shape and the goal is to estimate the value of τ by analysis of the received waveform $y(t)$, given by

$$y(t) = u(t-\tau) + noise \tag{8}$$

A predicted $u(t)$, as a template, is available for comparison with $y(t)$ at the receiver. It is assumed that τ is independent of time which means the target is stationary, and also it will be assumed that all the noise in the system, including that which is introduced by the receiver itself while operating on $y(t)$, can be regarded as an addition to the input signal.

Equations (7) can be rewritten as

$$p\ (\tau \mid y) = kp(\tau)\exp\{-\frac{1}{N_0}\sum_t u^2(t-\tau)\}\exp\{\frac{2}{N_0}\sum_t y(t)u(t-\tau)\} \tag{9}$$

Equation (9) shows that to estimate the delay, it is sufficient to calculate the convolution of $y(t)$ and $u(-t)$ - that is a cross correlation. None of the remaining terms involve $y(t)$.

The importance and effectiveness of cross correlation is shown in Fig. 7. Fig. 7 (a) shows a typical sample of Gaussian noise. The noise was constructed using a random function. The signal chosen is shown in Fig. 7 (b) which is real data captured by advanced sonar ring. As shown in the figure, $u(t)$ is delayed by an amount τ_0 which represents the TOF for the target. The sum of noise and signal, $y(t)$, is shown in Fig. 7 (c). $u(t)$ and $y(t)$ are available at the receiver, but $u(t-\tau_0)$ as shown if Fig. 7 (b), is not. The problem is to estimate where $u(t)$ is located in the noise.

Estimation process starts with

$$q(\tau) = \frac{2}{N_0}\sum_t y(t)u(t-\tau) \tag{10}$$

$q(\tau)$ has been computed over as wide range as possible, as shown in Fig. 7 (d). It will be seen that $q(\tau)$ has reduced the bandwidth of the noise so that it has a similar structure to that of the signal. In fact, this is because of cross-correlation process, which is an effective filter.

In Fig. 7 (e), the exponential function of $q(\tau)$ is plotted against τ, and if the prior distribution $p(\tau)$ is uniform, this final graph represents the complete expression (9) for $p\ (\tau \mid y)$.

It will be seen that all the posterior probability is concentrated in a narrow region of uncertainity at approximately the true value of τ. Actually, due to sampling effects and noise, the maximum of $p\ (\tau \mid y)$ does not fall exactly at the true value shown in Fig. 7 (b). In fact, one of the important factors in this process is signal/noise energy ratio that affects the uncertainity of the delay estimation.

3.2. Modeling Templates

A prediction of the received pulse shapes is needed to perform the cross-correlation. An accurate pulse prediction assists in achieving accurate TOF estimates. Furthermore, an accurate pulse prediction enables confident identification of sonar pulses from signal contaminated by considerable noise. Modeling templates is therefore considered important for robustness and performance of the sonar ring. The sonar pulse depends on many factors which must be taken into account to accurately predict its shape. Most important factors are the transducer characteristics, the excitation signal applied to the transmitter, the bearing angles at which the sonar wave front strikes the transducer, the dispersion and the absorption of air and the properties of the reflector.

To predict the template pulse shape, these effects are incorporated into a physical linear model [11]. The anticipated signal at the receiver, $rec(t,\theta_r,\theta_R,r)$, for a transmitter excitation $s(t)$ is given by

$$rec(t,\theta_r,\theta_R,r) = s(t-\frac{r}{c}) * h_{trans}(t,\theta_T) * \frac{1}{\rho} h_{air}(t,r) * h_{refl}(t) * h_{rec}(t,\theta_R) \tag{11}$$

where h_{trans} is the impulse response of the transmitter, h_{air} is the impulse response of sound in air, h_{refl} is the impulse response of the reflector and h_{rec} is the impulse response of the receiver. In equation (11), the "*" represents the convolution operator. The distance r is the total distance of flight to and from the reflector. The angle θ_r is the angle at which the sonar pulse emanates from the transmitter and θ_R is the angle at which the sonar pulse approaches the receiver.

Since air is assumed to be a linear medium, the following property holds

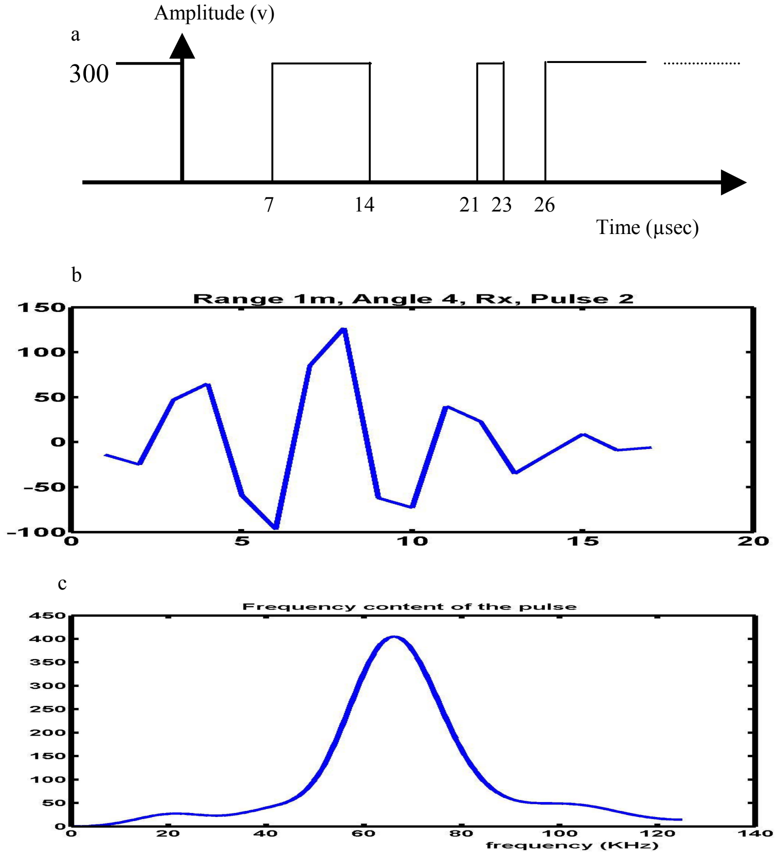

Figure 8. (a) voltage waveform to drive transmitters (b) an echo (c) frequency components of the echo

$$h_{air}(t, r_1 + r_2) = h_{air}(t, r_1) * h_{air}(t, r_2) \tag{12}$$

The transducers are much further from the reflector compared to the size, and therefore the impulse response due to the transmitter and receiver can be further refined as

$$\begin{aligned} h_{trans}(t, \theta_T) &= h_\theta(t, \theta_T) * h_T(t) \\ h_{rec}(t, \theta_R) &= h_\theta(t, \theta_R) * h_R(t) \end{aligned} \tag{13}$$

where h_T and h_R are the impulse responses of the transmitter and receiver at normal angle of transmission and incidence. Note that the same impulse response, h_θ, due to angular dependence applies to transmitter and receiver, due to reciprocity between transmitter and receiver. From equations (11-13) can be rewritten as

$$rec(t, \theta_r, \theta_R, r) = ref(t - \frac{r}{c}) * h_\theta(t, \theta_T) * \frac{\rho_{ref} 1}{\rho} h_{air}(t, r - r_{ref}) * h_\theta(t, \theta_R) \tag{14}$$

where the reference pulse

$$ref(t) = s(t) * h_T(t) * \frac{1}{\rho_{ref}} h_{air}(t, r_{ref}) * h_{refl}(t) * h_R(t) \tag{15}$$

is created by a plane aligned in front of the transducer at a fixed reference distance r_{ref}. The reference pulse $ref(t)$ incorporates the time-invariant characteristics of the transmitter and receiver h_T and h_R. By assuming that all indoor reflectors have similar responses, the impulse response h_{refl} is implanted into reference pulse $ref(t)$. $h_{air}(t, r_{ref})$ and $1/\rho_{ref}$ represent the absorptive and spreading effects of air for the reference distance r_{ref}. Using the reference pulse and the impulse responses h_θ and h_{air}, the received pulse shape $rec(t, \theta_r, \theta_R, r)$ can be predicted from equation (14). Thus, to predict the received pulse shape, the impulse responses h_θ and h_{air} must be determined.

The angular impulse response h_θ can be obtained from the transducer shape. The received amplitude is proportion to the area exposed to the pressure impulse, and thus the response is the height profile as the impulse grazes past the surface at an angle α to the surface normal. For a circular transducer, the impulse response has the shape of the positive half of an ellipse with width equal to the propagation time across the face of the transducer, $t_w = D\sin(|\alpha|)/c$, where D is the transducer diameter. That is

$$h_\theta(t,\alpha) = \begin{cases} \dfrac{4c\cos(\alpha)}{\pi D \sin(|\alpha|)}\sqrt{1-(\dfrac{2t}{t_w})^2} & ,-\dfrac{t_w}{2} < t < \dfrac{t_w}{2} \\ 0 & ,otherwise \end{cases} \qquad (16)$$

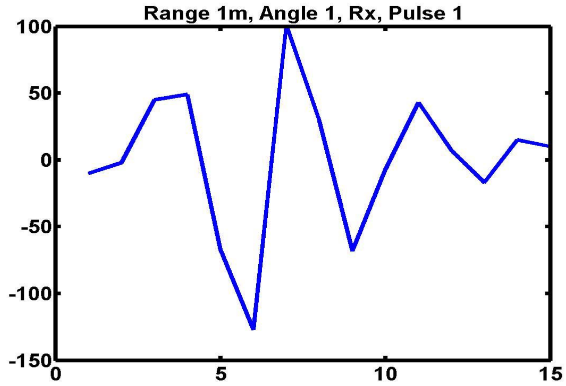

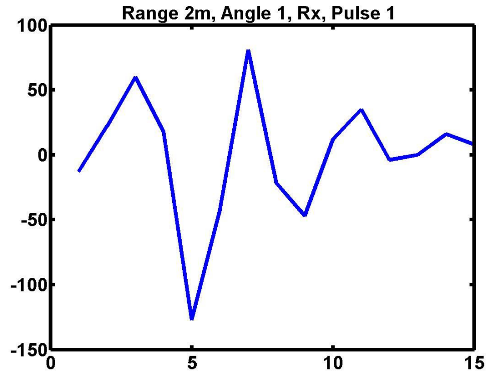

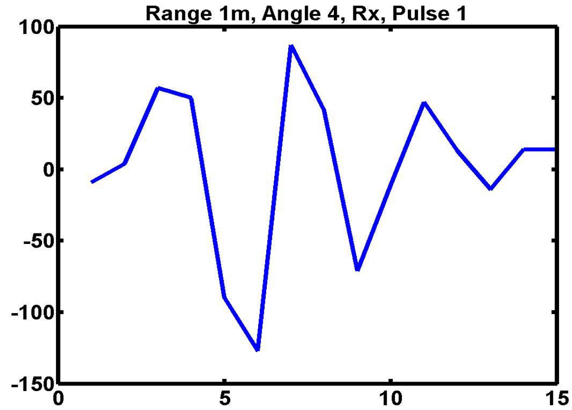

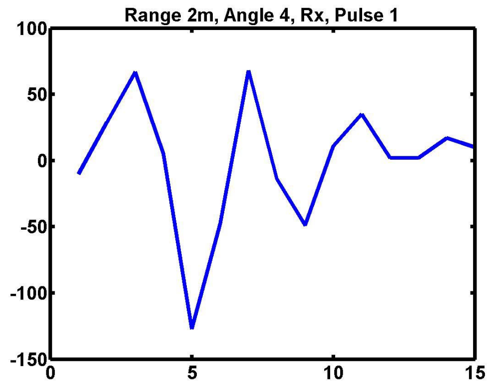

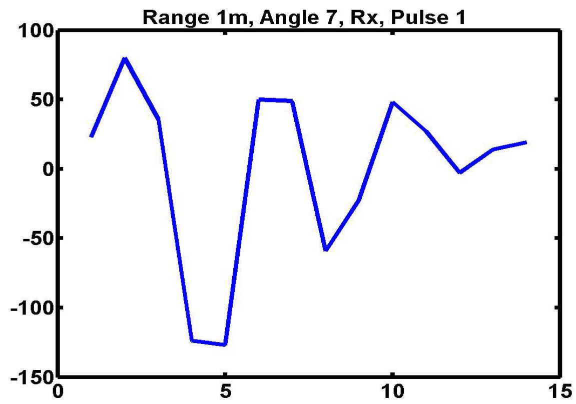

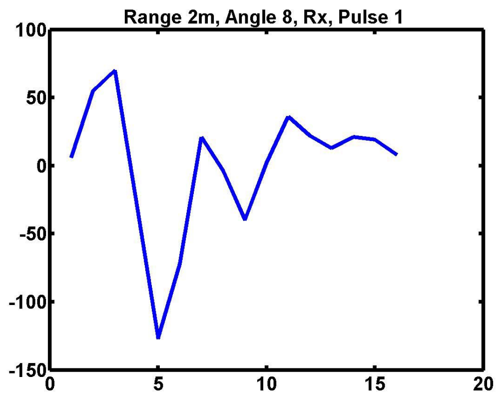

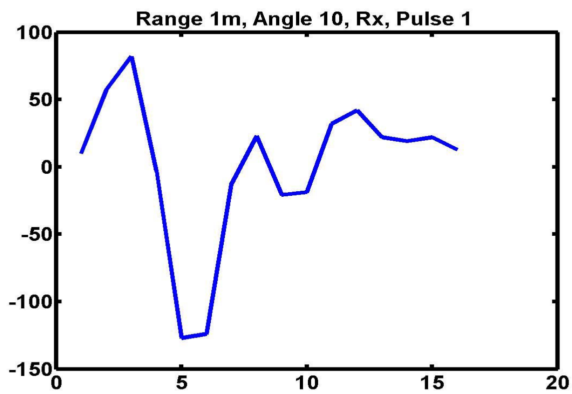

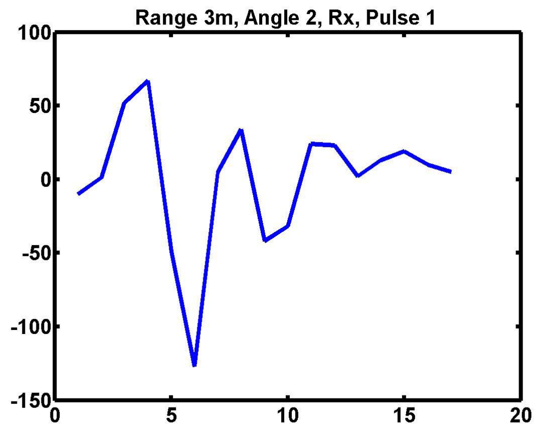
Range 3m, Angle 2, Rx, Pulse 1


Range 3m, Angle 6, Rx, Pulse 1

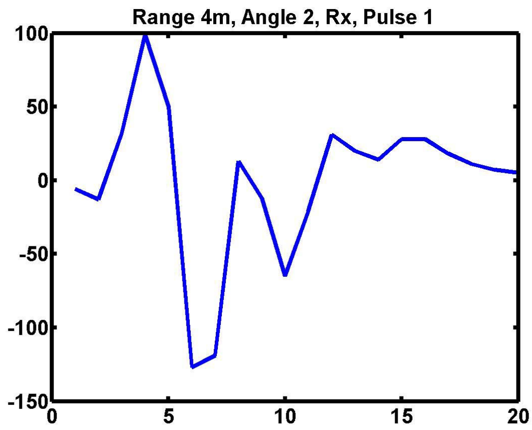
Range 4m, Angle 2, Rx, Pulse 1

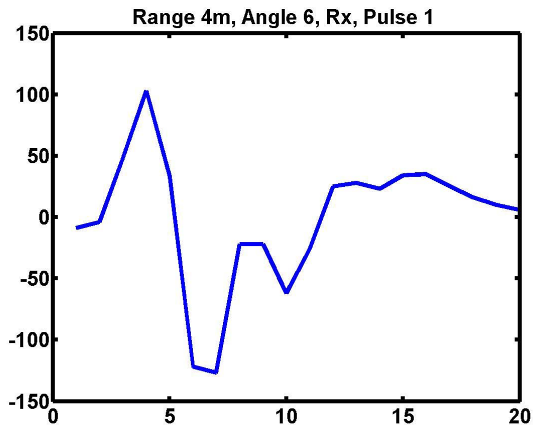
Range 4m, Angle 6, Rx, Pulse 1

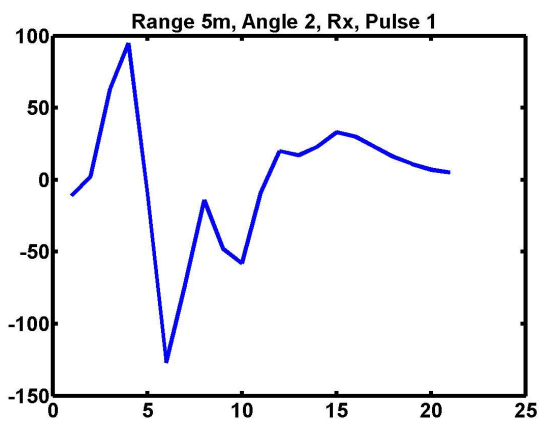
Range 5m, Angle 2, Rx, Pulse 1

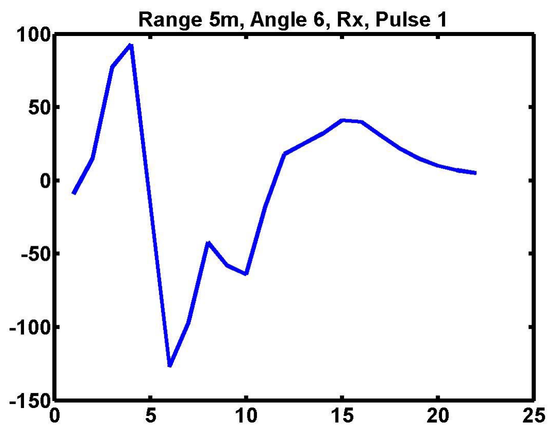
Range 5m, Angle 6, Rx, Pulse 1


Range 1m, Angle 1, Trx, Pulse 1
150
100
50
0
-50
-100
-150
0
5
10
15
20


Range 1m, Angle 4, Trx, Pulse 1
100
50
0
-50
-100
-150
0
5
10
15
20

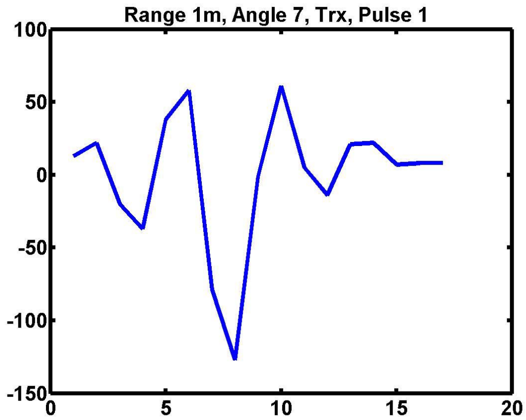
Range 1m, Angle 7, Trx, Pulse 1
100
50
0
-50
-100
-150
0
5
10
15
20

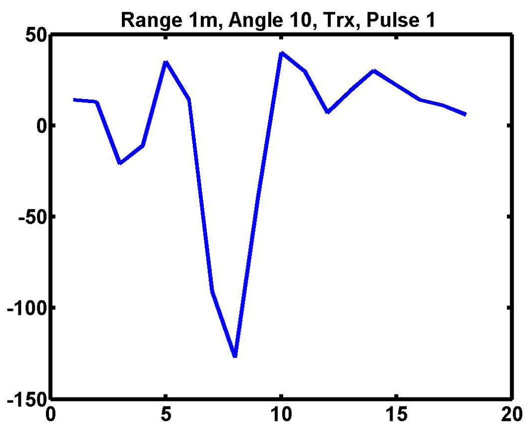
Range 1m, Angle 10, Trx, Pulse 1
50
0
-50
-100
-150
0
5
10
15
20

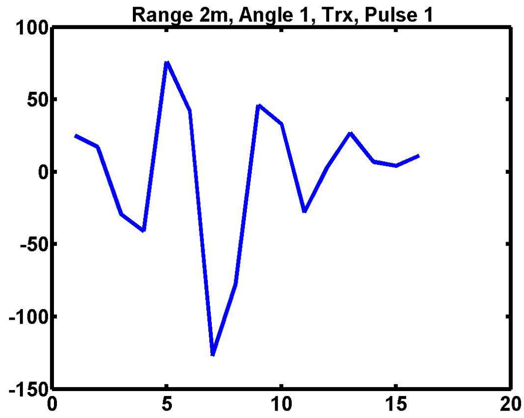
Range 2m, Angle 1, Trx, Pulse 1
100
50
0
-50
-100
-150
0
5
10
15
20


Range 2m, Angle 4, Trx, Pulse 1
100
50
0
-50
-100
-150
0
5
10
15
20

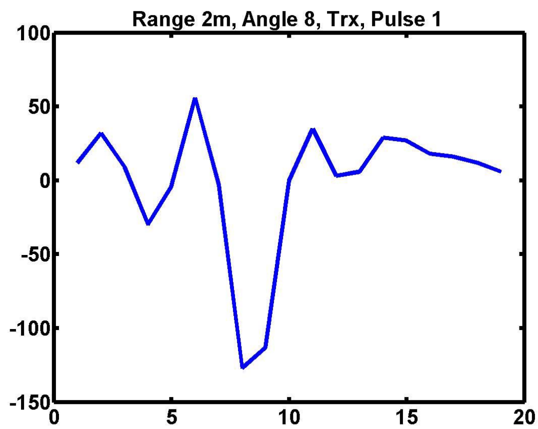
Range 2m, Angle 8, Trx, Pulse 1
100
50
0
-50
-100
-150
0
5
10
15
20

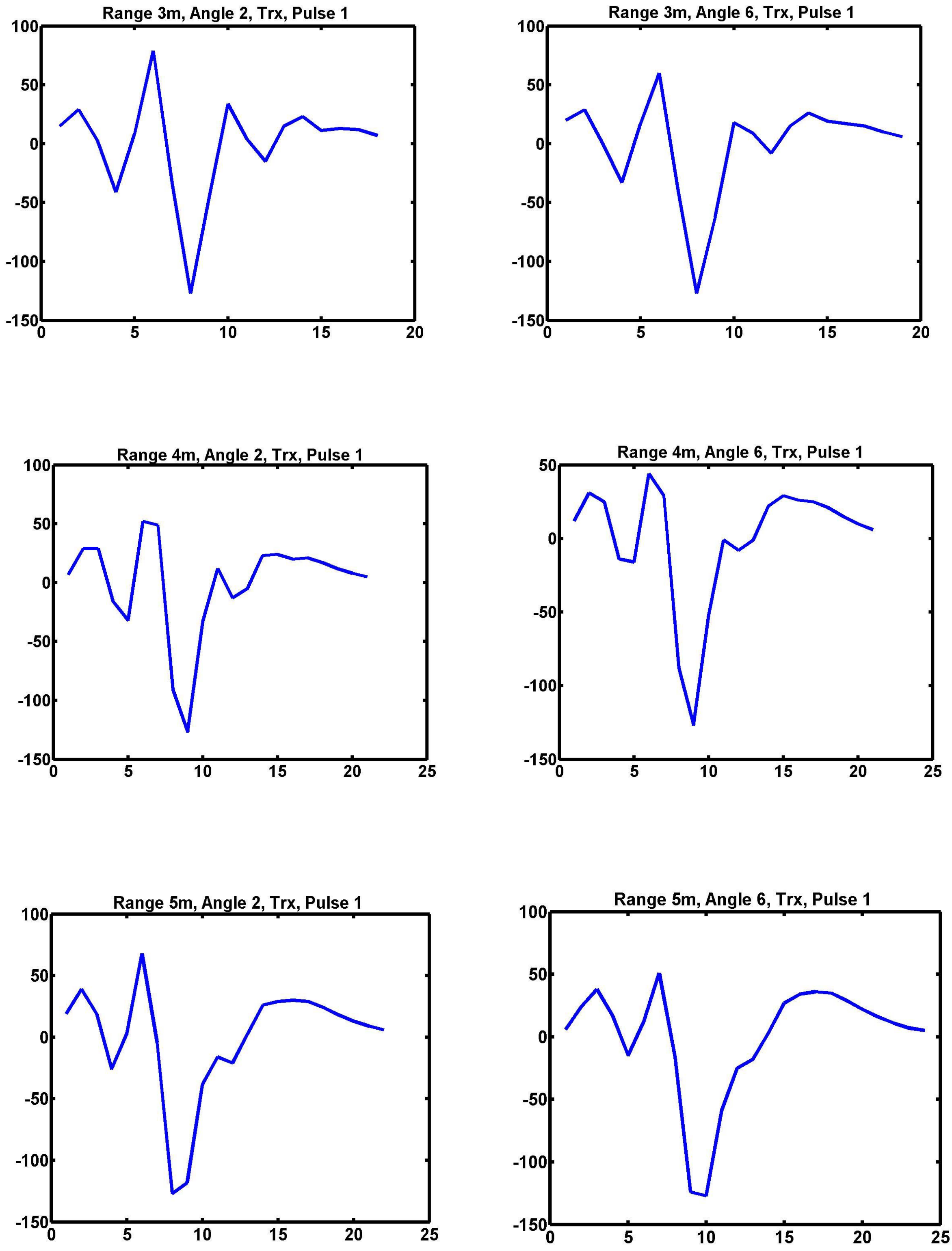

Figure 9. Two Sets of 13 Matched Filter Templates for Receivers and Transceivers of the Advanced Sonar Ring

As the distance to targets is usually much greater than the transmitter to receiver separation, the angles θ_R and θ_r are considered to be equal. Consequently, the angular response of the transmitter and receiver are combined to give

$h_\theta * h_\theta$ which is simply dependent on the single angle θ. However, when targets are close to sensor, the angles θ_R and θ_r may be sufficiently different to warrant individual attention.

The air propagation medium absorbs sound energy as a complicated function of temperature, humidity and frequency due to spreading and absorption. The spreading reduction of the energy density is governed by the inverse square law. As air is not a perfectly static medium, a portion of the propagating sound wave's energy is absorbed. In this work, we use the approach of Kleeman and Kuc [11,12] in estimating the absorption as a function of frequency and apply it to estimate the impulse response of sound in air h_{air}.

The sonar ring simultaneously fires all 24 transmitters of the ring using a very short square-wave pulse, and analysis simultaneously the waveforms at all 48 receivers using matched filters to accurately determine the arrival time of echoes.

The transmitted pulse is 2 cycles of 71.4 KHz plus a counter-timed burst to reduce reverberation in the transducer. The pulse is generated by momentarily removing a 300V bias, the same as is required to operate the transducers as receivers. Fig. 8 shows the voltage waveform used to drive transmitters, a sample waveform received from a smooth, hard reflector and the frequency components of the echoed signal using fast Fourier transform (FFT). A template for one metre range and zero bearing was used as a prototype, and above mentioned physical models were applied to generate the templates shown. The pulse absolute amplitude is normalised to maximum of 127, so the waveforms can be stored in an array of signed bytes. Multiple matched filters are required to maintain accuracy because the pulse shape depends greatly on the bearing of the reflector and its range. In fact, this dependence has been utilised for direct bearing measurement [19].

Due to different electronic circuits applying to transceivers and receivers of the advanced sonar ring, the echo pulse shapes of the same target are slightly different and therefore it is necessary to make particular sets of templates for each of them to gain the highest cross correlation (Fig. 9). Reflections from long range at large angles are unlikely to be detected, and are omitted from the template set. By symmetry, positive and negative angles are indistinguishable.

Because pulse shape depends on range and angle of arrival, several filters are generated. The templates are pre-computed and saved in the DSPs. Finally 13 templates for each set are generated for varying ranges and angles that includes for one metre range, one, four, seven and ten degrees bearing, for two metre range, one, four and eight degrees bearing, for three metre range, two and six degrees bearing, for four metre range, two and six degrees bearing and for five metre range, two and six degrees bearing (Fig. 9).

3.3. Estimating the TOF

Based on section 3.1, the maximum likelihood estimator for the arrival TOF with additive white Gaussian noise is the time τ that maximizes the cross-correlation, $Cor(\tau)$, between the received pulse $p(t)$ and an anticipated pulse shape $ant(t)$.

$$Cor(\tau) = \frac{\sum_T p(t)ant(t-\tau)}{\sqrt{\sum_T p^2(t)\sum_T ant^2(t)}} \tag{17}$$

The anticipated pulse shape $ant(t)$ is one of the templates shown in Fig. 9 captured from a plane in one metre range and one degree bearing. The received echo is tried against all available templates for several different angles at the given range, and the one which gives the highest correlation coefficient is selected to estimate the arrival time. A sonar pulse is registered if its maximum cross-correlation is greater than 80% otherwise is discarded. There are some reasons why a pulse may be rejected including environmental noise, another sonar sensor using a different pulse shape, another transmitter in the same sonar ring using different pulse shape or overlapping pulses from different sources, resulting a distorted pulse.

To estimate the TOF to sub-sample accuracy (less than 4 microseconds in the advanced sonar ring), parabolic interpolation is performed on the maximum three adjacent samples of $Cor(\tau)$. If the three maxima y0, y1, and y2 occur at integer sample numbers 0, 1 and 2, the parabolic estimate of the position of the maximum is

$$new\_\max\_pos = prev\_\max\_pos - 1 + \frac{y_2 - 4y_1 + 3y_0}{2(y_2 - 2y_1 + y_0)} \tag{18}$$

where $prev\_\max\_pos$ is the position of y1 and $new\_\max\_pos$ is the new maximum position with sub-sample resolution.

TOF is determined by applying matched filtering to the echoes identified by thresholding and pulse splitting. Filtering is performed by first choosing a set of appropriate templates using the start sample number of the echo and finding the approximate range of the echo, then cross correlating the received echo with all selected templates. For example if the start sample number of the echo shows an approximate range of 120cm the first four templates are chosen by software. The alignment between the echo and each template are adjusted by 13 samples which means alignment of the peaks on each other and six shifts to each side, to maximize the correlation coefficient and to find the accurate maximum location in the echo. This is less comprehensive than a full convolution implementation but is advantageous as it can run faster and because each DSP processes all echoes of eight receivers, the process is computationally intensive.

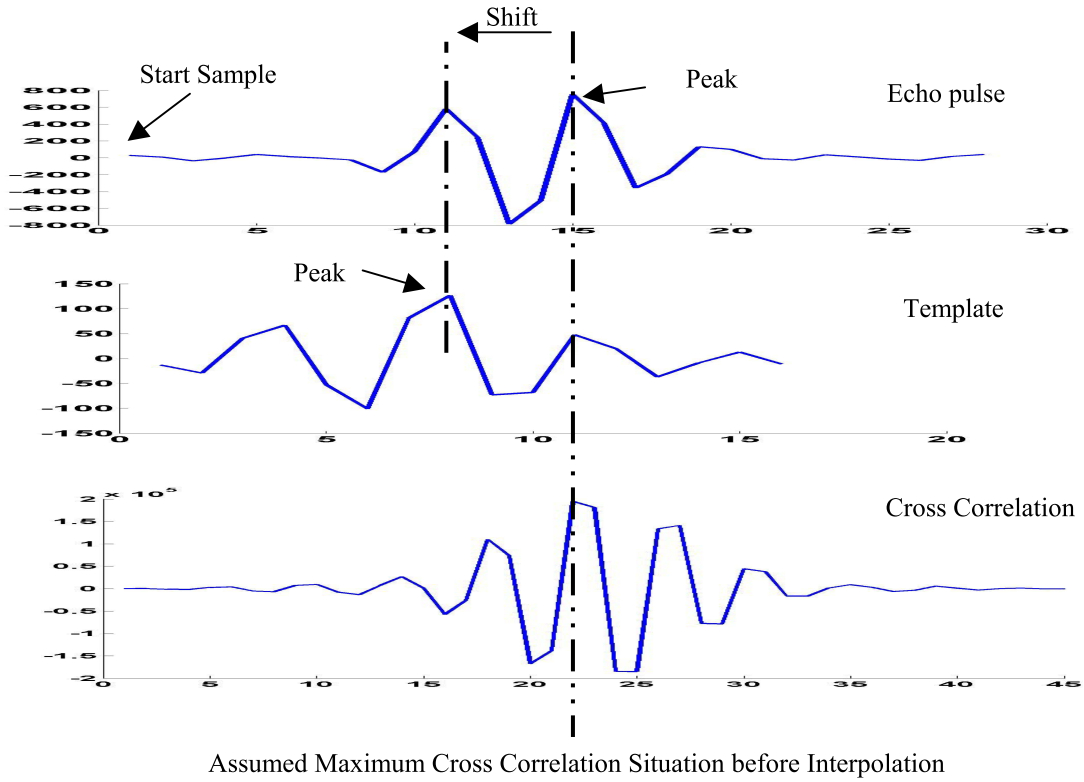

Figure 10. Alignment of a Received Echo and a Template when Maximum Correlation Occurs

After finding a reliable echo, exceeding the correlation threshold, which is 80%, the question is how to calculate the TOF. In fact, the TOF is the start point of the echo pulse, but noise can change the start point of the echo and more importantly in practice the thresholding and splitting process, as are explained later, relies on groups of eight samples that at least one of them exceeds the threshold level, therefore the registered start point of the echo varies with time and can not be considered as a reliable TOF.

The method used in the advanced sonar ring is to find the start point of the template when the alignment of template and pulse results the maximum correlation. Fig. 10 shows an example of filtering, assuming in this condition, maximum correlation happens, therefore the TOF is

$$TOF = 4\mu\sec(pulse\_peak\_no - template\_peak\_no - shift) \tag{19}$$

where $pulse\_peak\_no$ is sample number of the pulse peak and $template\_peak\_no$ is the sample number of the template peak, and in the calculation of the $shift$, sub sample resolution is considered using equation (18).

$$shift = peak\_dif - (-1 + \frac{y_2 - 4y_1 + 3y_0}{2(y_2 - 2y_1 + y_0)}) \tag{20}$$

where $peak\_dif$ is difference between $pulse\_peak$ and $template\_peak$ when maximum correlation occurs (Fig. 10).

3.4. Estimating the Bearing to Targets

The advanced sonar ring includes 24 pairs of transducers, and in each pair one transducer acts as transceiver and another as receiver. To derive the bearing angle to a physical target, a pulse must be received and accepted on both of the receivers of each pair, and correctly associated with each other and the physical reflector. Because the receiver physical spacing is just d=40.5 mm, the correspondence problem is usually easy to solve, and is simply based on matching the arrival times and pulse amplitudes within predefined ranges. If only both correlation coefficients are over 80% and the ratio of pulse amplitudes is between 0.5 and 2.5 and arrival times differ by less than $d\sin(\max\_angle)/c$=20µsec which is consistent with transducers physical spacing, the association is flagged reliable, otherwise it is considered as unreliable and the information may be used for collision avoidance or further process.

Fig. 11 shows one transceiver Trx and one receiver Rx of a pair of transducers separated by a distance d which is 40.5mm in the advanced sonar ring. The range from the reflector R to the two transducers are r_{Trx} and r_{Rx}. The bearing angle to the transmitter, θ is determined using the cosine rule.

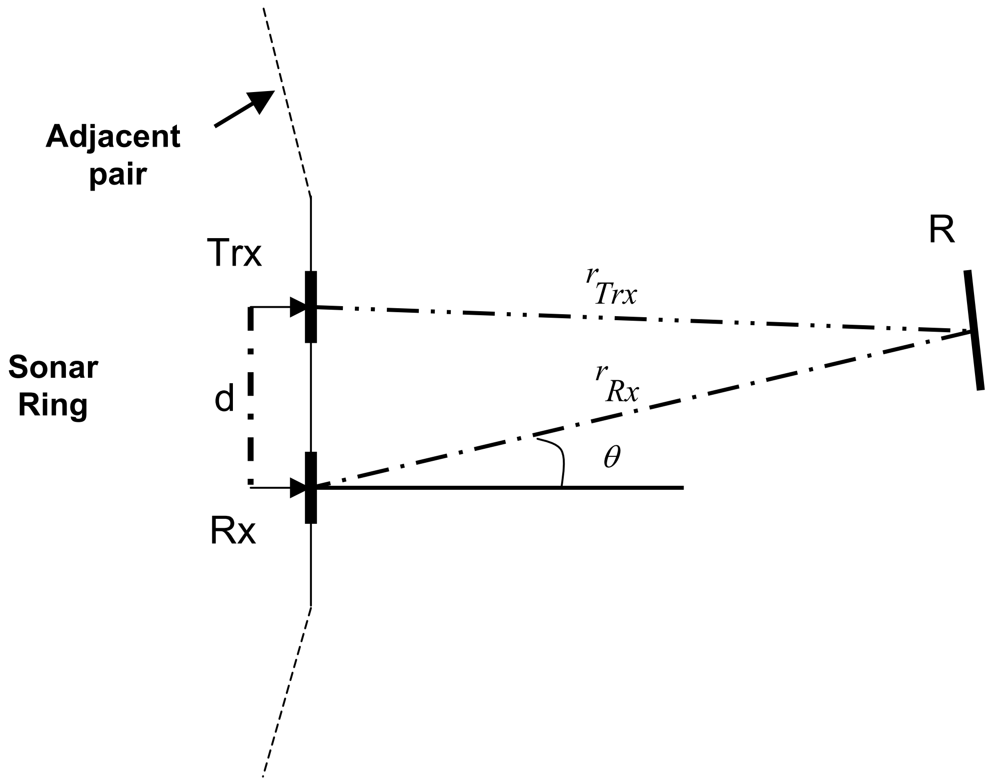

Figure 11. Bearing Calculation

$$\theta = \frac{\pi}{2} - \cos^{-1}\left(\frac{d^2 + r_{Rx}^2 - r_{Trx}^2}{2dr_{Rx}}\right) \tag{21}$$

4. The Advanced Sonar Ring Software Architecture

The software consists of three parts, a host program, a master program and a slave program. The host program is developed using C++ under Linux which provides a graphical user interface to communicate with the sensor using a serial port, and to save the results while showing them in the screen. A user is able to send different commands to the sensor, such as upload and download of data memory and program memory of master DSP and slave DSPs, firing of transducers, reading and writing of the flash memory and transferring the high level data to the host, shown in the graphical environment.

The master and slave programs are stored in the flash memory. After turning on the sensor, the master is booted via the byte DMA method of ADSP-2189M. This software is a command parser capable of communication with the host computer and all digital slave boards, allowing the central computer to control all parts of the advanced sonar ring. By sending a command to the master, it can boot all digital slave boards using internal DMA port. A fire command is issued to all slaves simultaneously, thus synchronizing the firing of all transceivers to within a clock cycle or 13 nanoseconds. The software of each slave can communicate with the master by a command parser containing some commands to access low level data. The most important part of this software is an echo processor that is organised into two phases. During the first stage, assembly code performs on-the-fly processing of the samples from the eight receivers to extract discrete pulses that exceed the noise floor. On-the-fly processing is essential not only to have a real time sensor but also to conserve the on-chip data memory of the DSP. The second stage processes the extracted pulses with C code to extract arrival times using matched filtering.

4.1. DSP Phase One Processing - Pulse Capturing

The phase 1 consists of highly optimised assembly code to extract pulses from eight receiver channels and save them into pulse buffers. This real time program enables approximately 128k words of raw receiver data to be processed in a transmit cycle to yield pulse results within the 48k words of data memory. The software is run while receiving echoes and processes all eight channels within 150 instruction cycles or two microseconds. This phase has a main program and a timer interrupt routine that runs every two microseconds. Each slave board contains two 4-channel ADCs producing multiplexed 2+2 data. The timer interrupt routine fetches the next 12 bit ADCs samples from the eight receiver channels and places them into eight circular buffers. Therefore the sampling rate for each receiver channel is 250 kHz. The interrupt routine is also responsible for generating the transmit pulse.

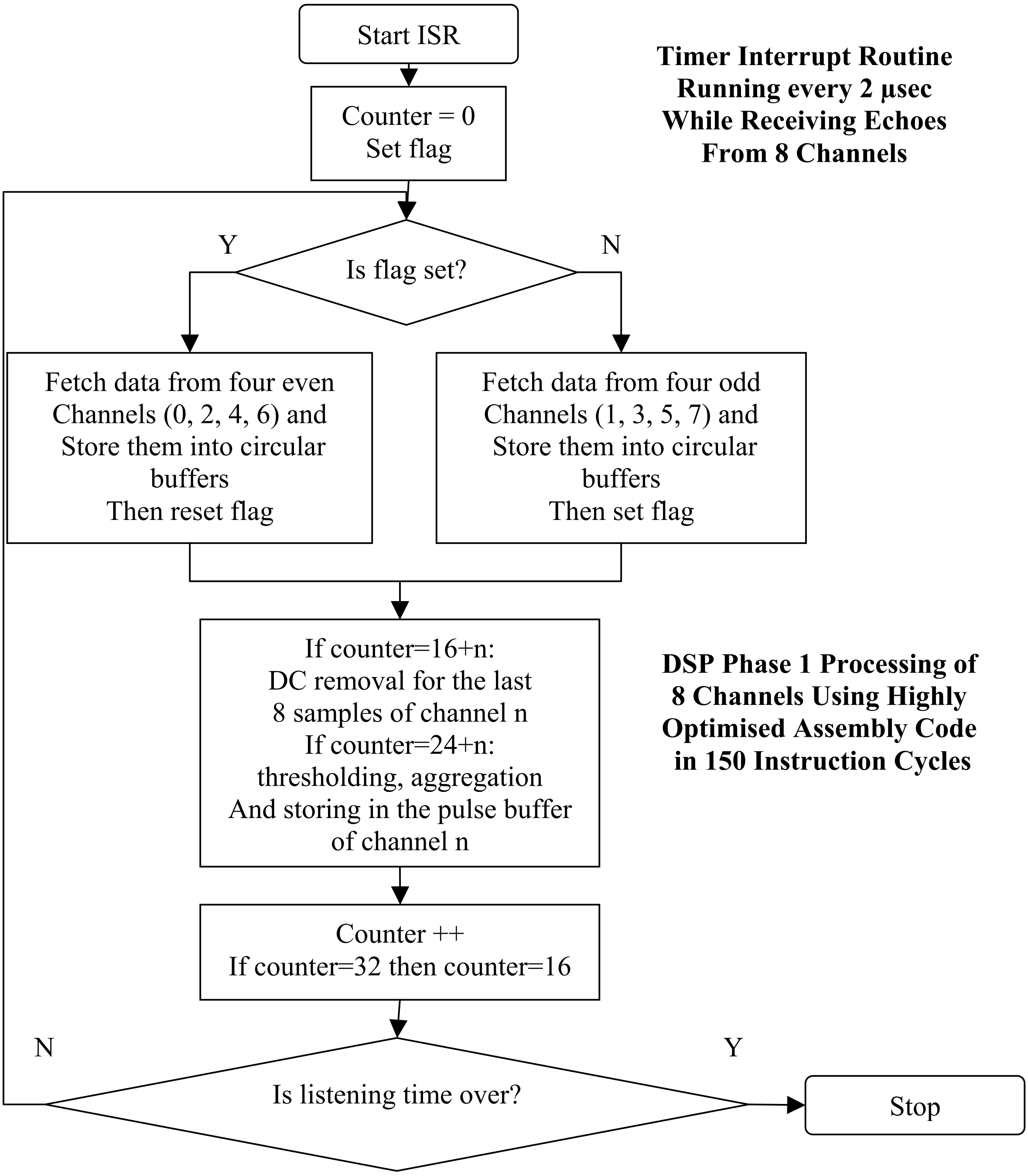

Figure 12. Phase One Processing Flow chart

The main program runs in a loop where each iteration processes the block of data acquired since the previous iteration. The phase 1 processing occurs concurrently with respect to the capture time and consequently must keep up with the incoming data to avoid buffer overflow errors. The eight channels are processed independently through four stages: DC bias removal, thresholding, aggregation and storing into a pulse buffer (Fig. 12).

- Filtering**:** An optimised high pass software filter removes the DC voltage of echo. This process operates in-place on data in each circular buffer [8].

- Thresholding**:** Each receiver sample is compared with a threshold to classify the sample as noise or part of an echo pulse. Since an echo pulse can legitimately pass through zero, a block processing technique is used. Each block of eight samples containing at least one sample with amplitude greater than the threshold are deemed to be part of an echo. An adaptive threshold level is applied to allow for different time varying gains in the receiver preamplifiers resulting in different noise levels. The threshold level is increased when the pulse buffer is fully occupied and is decreased when it is nearly empty. Due to limitation in size of each pulse buffer especially in a cluttered environment, this adaptive method is useful.

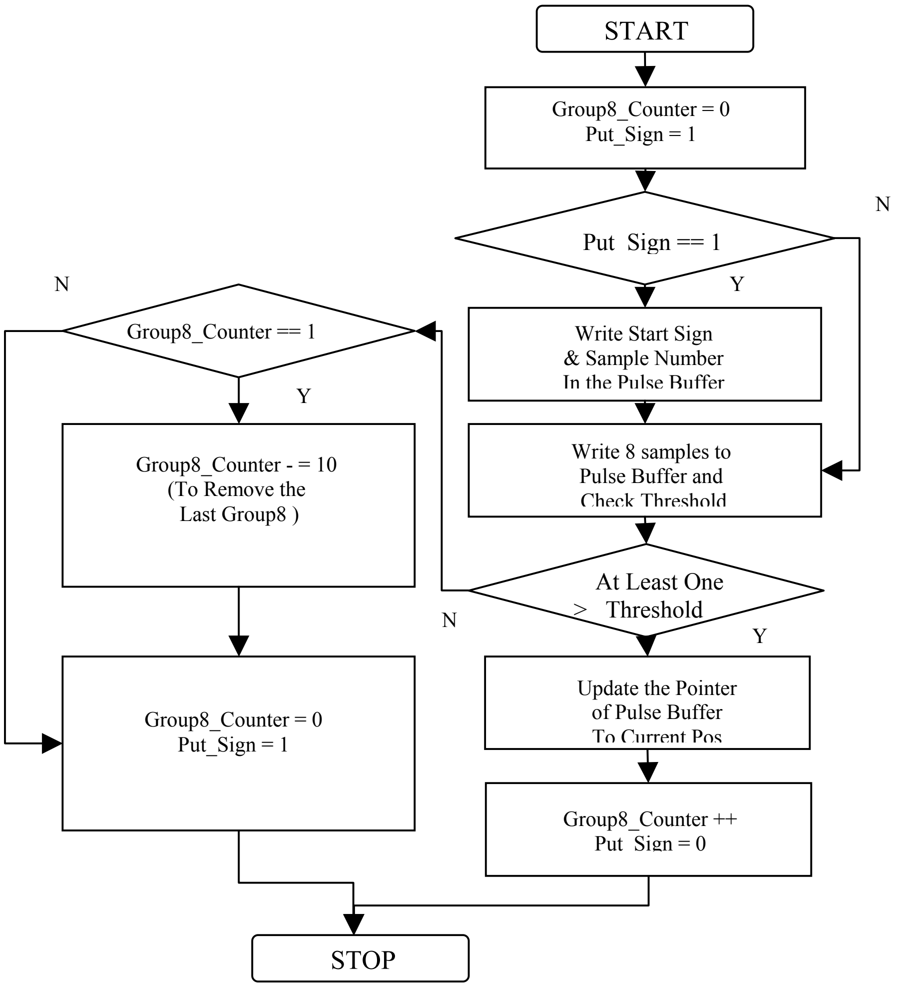

Figure 13. A Flow Chart of an On-The-Fly Thresholding , Aggregation and Storing Assembly Code for each channel

- Aggregation and Storing**:** When there are two or more consecutive blocks exceeding the threshold level, the software merges them along with the resulting ranges for later template matching. Each receiver channel has its own pulse buffer. Due to the transmitted pulse shape, the length of an echo should be greater than eight samples so a block of eight samples is deemed to be a noise. This reduces the time required for matched filtering in the next stage (Fig. 13).

4.2. DSP Phase Two Processing – Matched Filtering and Bearing Estimation

Phase two processing occurs in the DSP after all receiver channels have been logged and stored simultaneously in the pulse buffers. The processing time in this stage occurs in addition to the time of flight between transmitting and receiving the furthest echo – approximately 32 milliseconds. This processing time then directly impacts on the real time performance of the sensor since it takes place sequentially with respect to the capture time.

To determine the echo pulse arrival times, matched filtering is performed on the echo pulses extracted during phase one of the processing. Template matching obtains the arrival time by cross correlating the received echo pulse with an echo template stored in the DSP. A template is a noise free pulse shape computed offline from a calibration pulse obtained from a plane at one metre range straight ahead. The template is shifted across the echo to find the maximum correlation [8]. By finding a parabola to the maximum three correlations and their shift times, a very accurate arrival time as a fraction of the 4 microsecond sample time is estimated [11].

A complication in the template matching is that the pulse shape depends on the angle of arrival and the range. These templates for different ranges and angles can be computed offline [11]. For each metre of range several different template pulses are computed and stored within the DSP program memory corresponding to all the possible arrival angles. The DSP is capable of performing a very fast cross-correlation process. Matched filtering is tried across all possible angles at the given range and the highest match is selected to estimate an arrival time.

After all arrival times are estimated, the bearing estimation is performed for all targets seen by both receivers of each pair using an above mentioned triangulation method. If a target is seen by just one of the receivers it is deemed to be an unreliable target. At the end of the calculation, the slave boards are waiting to be read by the master board and after the high level data of all slave boards are read and sent to the central computer, the master board sends another fire command simultaneously to all the slave boards.

5. Experimental Results

5.1. Reference Point and Offset Table Concept and Results

Choosing a reference template amongst all precomputed templates is an important issue, which results the exclusive indication of the start point of an echo, matched with varying templates, that is the same TOF when maximum correlation occurs in different templates.

The importance is due to varying sizes and asymmetric pulse shapes of templates used in matched filtering. In other words, the TOF of a stationary target or a very slow object, when maximum correlation occurs with different templates in matched filtering, in the templates of the same range or different ranges, is varying because of the different start points of templates.

In the advanced sonar ring, to solve this problem and avoid jumping TOFs, the template for one metre range and one degree bearing is selected as reference template and the start point of that is considered as the reference point of echoes .

The software uses a lookup table called offset table that contains offset values between the reference template and all others. To calculate the offset value, correlation between each template and the reference template is calculated and when maximum correlation occurs, the difference between two start points is calculated and considered as the offset value of that template (Fig. 14). To get sub-sample resolution the above mentioned interpolation method is also used in offset values computation. The offset table is pre-computed and saved with templates. Using offset values the equation (19) can be rewritten as

$$TOF = 4\mu\sec(pulse\_peak\_no - template\_peak\_no - shift - offset) \tag{22}$$

As mentioned earlier, the concept of the offset is based on cross correlation between the reference template and other templates, if the maximum occurs in the middle of the range, it will result a zero offset value, otherwise, the difference between start points of the reference and a template is considered as an offset. Now let us explain the basic theory of the offset concept. The process of offset calculation starts with

$$ref(t) \otimes template(t) \tag{23}$$

where $ref(t)$ is the reference template, which is the template of one metre range and one degree bearing, $template(t)$ is another template and the operator $\otimes$ is used for cross correlation. Using equation (14), the expression (23) can be rewritten as

$$\begin{cases} ref(t) \otimes (ref(t) * h_\theta(t) * h_\theta(t)) & ,for\ \ one\ \ meter\ \ templates \\ ref(t) \otimes (ref(t) * h_\theta(t) * h_\theta(t) * h_{air}(t)) & ,other\,templates \end{cases} \tag{24}$$

It can be proved that

$$f(t) \otimes (g(t) * h(t)) = (f(t) \otimes g(t)) * h(t) \tag{25}$$

where

$$\begin{aligned} f(t) * g(t) &= \int_{-\infty}^{+\infty} f(\tau) g(t-\tau) d\tau \\ f(t) \otimes g(t) &= \int_{-\infty}^{+\infty} f(\tau) g(t+\tau) d\tau \end{aligned} \tag{26}$$

To prove the equation (25) we start from right side

$$(f(t) \otimes g(t)) * h(t) = \int_\tau (f \otimes g)(\tau) h(t-\tau) d\tau = \int_\tau \int_\theta f(\theta) g(\tau+\theta) d\theta h(t-\tau) d\tau = \int_\theta f(\theta) \int_\tau g(\tau+\theta) h(t-\tau) d\tau \ \ d\theta \tag{27}$$

We consider $\tau+\theta$ as a new τ then

$$= \int_\theta f(\theta) \int_\tau g(\tau) h(t-\tau+\theta) d\tau\, d\theta \tag{28}$$

Swapping θ and τ , the equation (28) can be rewritten as

$$= \int_\tau f(\tau) \int_\theta g(\theta) h(t-\theta+\tau) d\tau\, d\theta = \int_\tau f(\tau)(g*h)(t+\tau) d\tau = f \otimes (g*h) \tag{29}$$

Using equation (25), the equations (24) can be rewritten as

$$\begin{cases} (ref(t) \otimes ref(t)) * h_\theta(t) * h_\theta(t) & ,for\ \ 1\ \ m\ \ templates \\ (ref(t) \otimes ref(t)) * h_\theta(t) * h_\theta(t) * h_{air}(t) & ,other\,templates \end{cases} \tag{30}$$

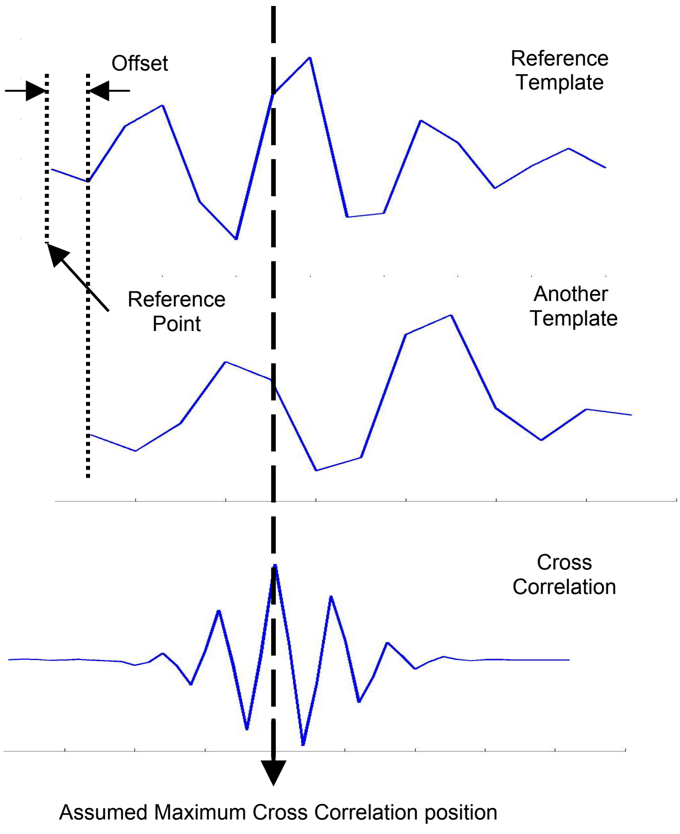

Figure 14. The Concept of the Offset and Calculation Method

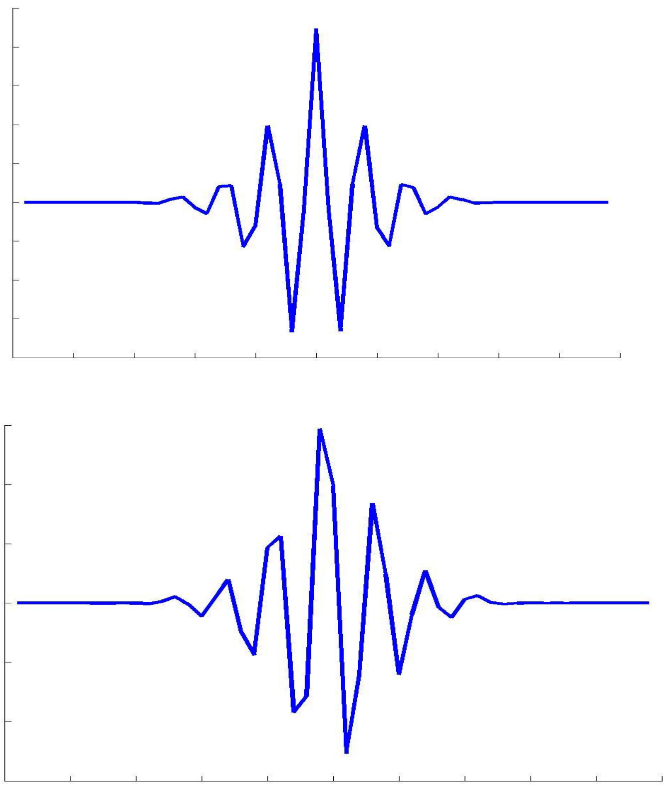

Figure 15. Cross Correlation of the Reference Template with Another One Meter Template (up) and a Two Meter Template (down)

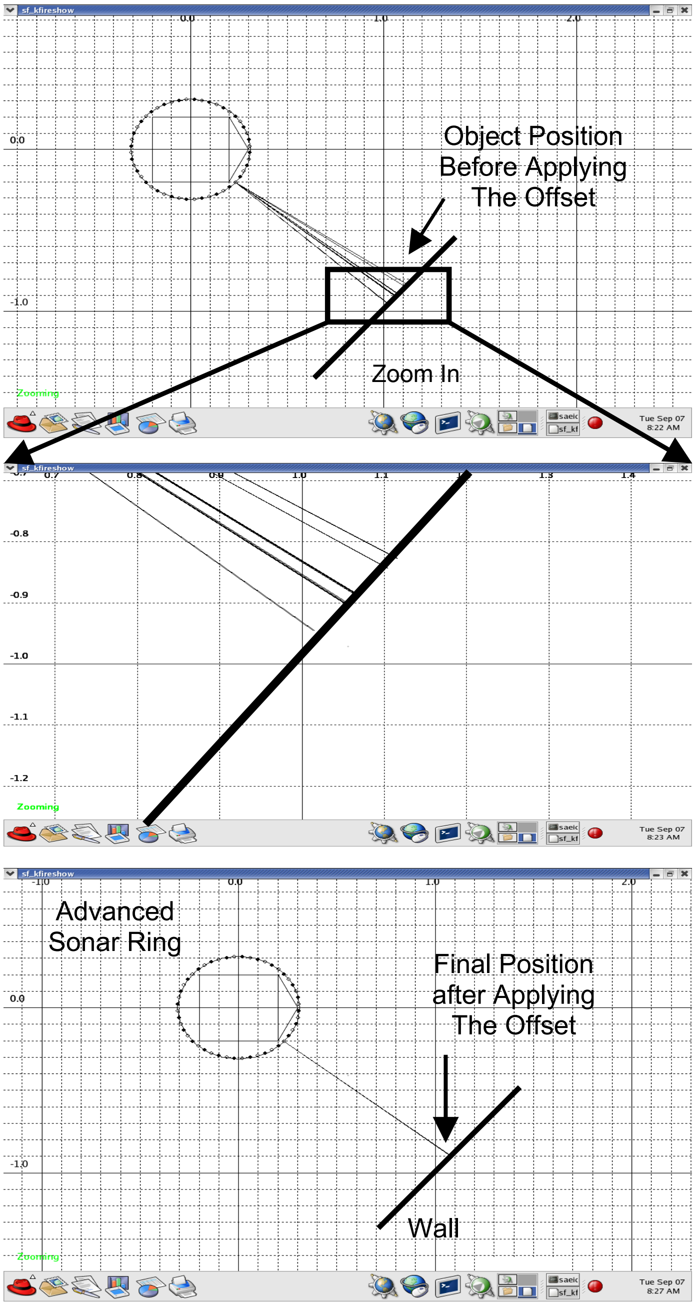

Figure 16. Experimental Result of a Wall position befor and after Applying the Offset

where the term

$$ref(t) \otimes ref(t) \tag{31}$$

is called auto correlation of the reference template, and it can be proved that it is an even function, maximized at the origin which means

$$\int_{-\infty}^{+\infty} ref(\tau)ref(t+\tau)d\tau \;\; <= \;\; \int_{-\infty}^{+\infty} ref^2(\tau)d\tau \tag{32}$$

the other term

$$h_\theta(t) * h_\theta(t) \tag{33}$$

based on Equation (16), is auto convolution of an even function which is the same as auto correlation and results another even function, maximized at the origin. Therefore, theoretically, for one metre templates, the maximum correlation occurs at the origin resulting zero offset value, but for other templates due to term $h_{air}(t)$, which is not an even function, the maximum correlation may occur at the point shifted from the origin, resulting non-zero offset value. Fig.15 shows the result of cross correlation between the reference template with another one meter range template which results an even function and with a two meter range template which does not result in an even function. In the advanced sonar ring, because we truncate all the templates from both sides after convolution with h_θ , the offset values are non-zero even for one meter templates. This truncation, firstly minimizes the sizes of the templates and makes it possible to save them in the DSP memory, and secondly increases the speed of the template matching process.

When the offsets are not applied, the result of range estimation for a stationary target such as a wall is not consistent and different ranges are calculated when the maximum correlation occurs with different templates. The experimental results, before and after applying this factor are shown in Fig. 16. This problem also occurs when a calculation process of a moving platform or moving target uses different templates due to change in the given range, for example when it uses 1 metre templates and then changes to two meter templates. Therefore the offset table removes the source of these errors.

5.2. Cycle Hopping Rejection Concept and Results

The matched filtering is performed using a 13-point cross correlation, explained in section 3, between a determined echo and each of the related templates for a given range. If the maximum correlation is greater than 80% then the echo is considered as a reliable echo, then the arrival time of the echo is estimated using equation (22).

During experiments, we found the position of a stationary object sometimes jumps between two different positions. More investigation of the echoes showed that the maximum value of the cross correlation, which is sampled at the same rate of the echo, occurs in different locations within cross correlation vector, resulting a varying TOF value caused by a changing shift, described in equation (19). This problem is called cycle hopping since the error in shift is usually approximately one wavelength and details are shown in Fig. 17.

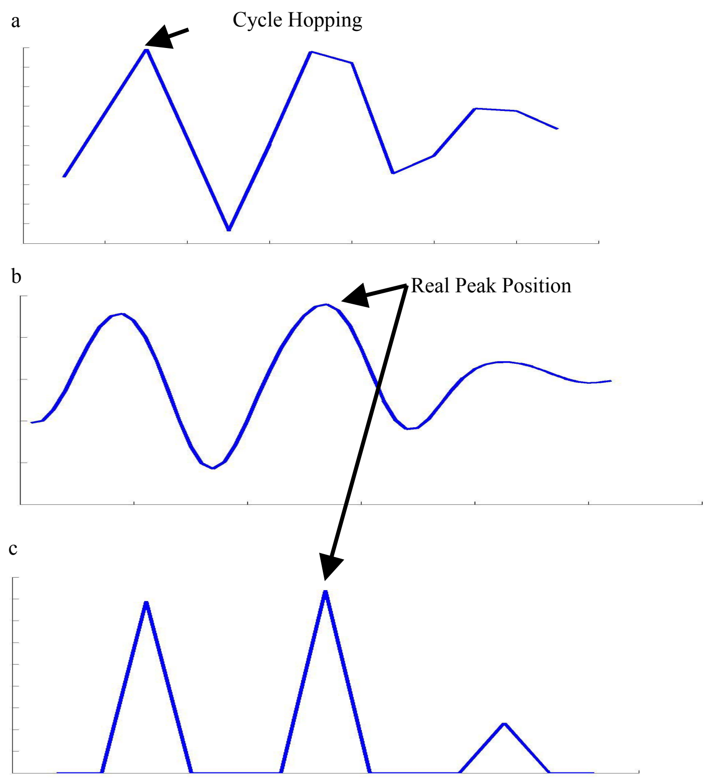

Figure 17. (a) A cross correlation at 250 kHz and the cycle hopping problem (b) the real shape of cross Correlatiom (c) real peak location using the interpolation method

The problem arises firstly due to a low sample rate of 250 kHz missing the real peak in the sampling process, and also due to the noise level in the captured echo, which makes local maxima very close to each other and indistinguishable in some conditions. Cycle hopping occurs when the amplitude of an adjacent local maximum is greater than that of the samples calculated around the real peak position.

To solve the problem and to find a genuine peak position within the cross correlation matrix, an interpolation process is employed after the cross correlation calculation. This process computes a real peak value of the local maxima using a parabolic interpolation over three adjacent samples. Then, the maximum is chosen amongst the results of this process.

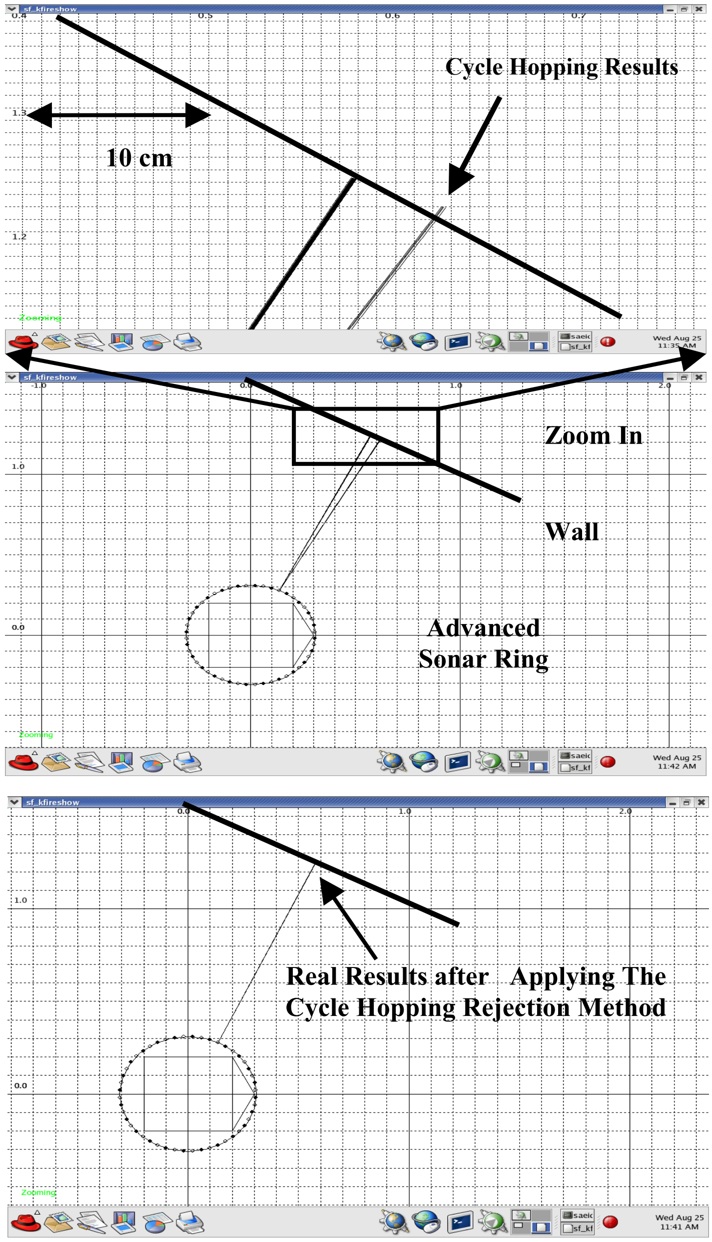

Figure 18. Experimental Data Showing the Effectiveness of The Cycle Hopping Rejection Method

Fig. 17 (a) shows a real cross correlation vector which has a peak in the wrong position, comparing to the other echoes captured from the same target and the same receiver. Fig. 17 (b) shows the real correlation waveform and the result of the interpolation process on the local maxima is shown in Fig. 17 (c). As can be seen, this method can provide a better estimate of the real maximum and avoid the varying TOF.

Also, experimental results are shown in Fig. 18. This figure shows the effectiveness of the applied method in the real environment. The computed position of each object is considered at the end of each line. The cycle hopping causes a difference of about 4 samples i.e. 16 microseconds in the arrival time of the echo, therefore about 16*0.343/2=2.75 mm difference in the range. As can be seen in Fig. 18, this variation effects the bearing estimation markedly when one of the ranges obtained from a receiver of each pair is fluctuating .

5.3. Target Association Results

To illustrate the DSP processing, the sonar ring was placed among a set of reflectors. The test environment consists of concave right angled corners and planes as shown in Fig. 19. Measured targets are shown as a line connecting a pair of transducers to the observed object.

The DSP sonar ring can be commanded to continuously report parameters on up to 20 pulses per receiver. Table I and II are these parameters in one position of the ring. The amplitude column represents the maximum amplitude of the pulse. Amplitude information is useful in classifying targets based on their reflectivity and also can be exploited in the association process discussed below. The correlation coefficient lies between –1 and +1 and is an important outcome of template matching [11]. It represents how well the received pulse matches the closest shaped template. A correlation coefficient above 80% indicates that a reliable arrival time has been obtained. Due to the slower sampling rate employed here of 250 kHz, the correlation coefficient is usually less than the correlations from a 1 MHz sample rate in [8]. Values below 80% are unreliable for bearing estimation purposes but still give an indication that an obstacle is present. In the current implementation, stage 2 processing can be performed in about 35 milliseconds for all receiver channels and this translates to a maximum sensor cycle time of 32+35 milliseconds or a 15 Hz repetition rate.

In order to derive the bearing angle to physical targets, pulse arrival times must be associated between the left right receiver channels in each pair of transducers. Ambiguities are possible in this process when there are many closely spaced pulses. Every pulse extracted from the left channel is compared with every pulse from the right. An association is declared reliable if both correlation coefficients are over 80% and arrival times are consistent with the receiver physical spacing (=40.5 mm) – that is arrival times differ by less than sin(max_angle)*40.5/speed_sound.

TABLE 1. RECEIVERS PULSE DATA FROM ENVIRONMENT

Transd. Pair no	Arrival Time (μsec)	Range (m)	Amp. (ADC counts)	Correl. Coeff %.
16	3482.035	0.591946	1492	87
19	5867.018	0.997393	1765	86
22	3768.959	0.640723	1514	86
23	4039.176	0.686660	1155	83

TABLE 2. TRANSMITTER/RECEIVERS PULSE DATA FROM ENVIRONMENT

Transd. Pair no	Arrival Time (μsec)	Range (m)	Amp. (ADC counts)	Correl. Coeff.
16	3482.112	0.591959	657	95
19	5867.759	0.997519	1082	92
22	3768.606	0.640663	757	95
23	4030.988	0.685268	977	90

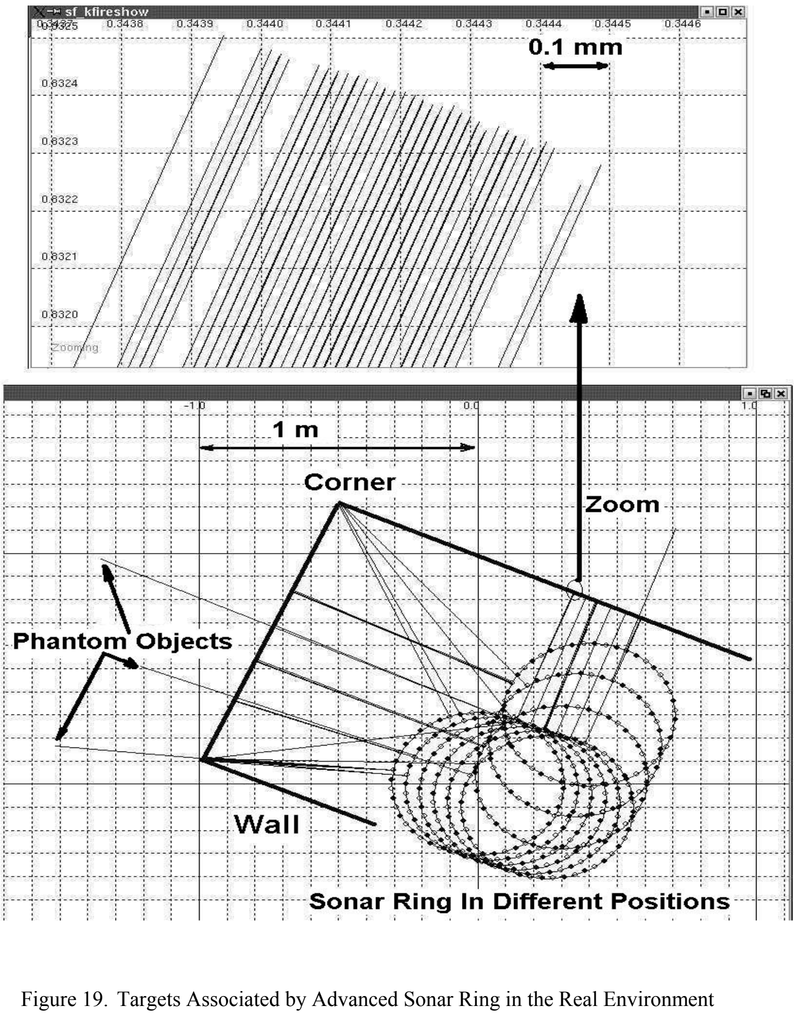

Figure 19. Targets Associated by Advanced Sonar Ring in the Real Environment

Fig. 19 shows results from different positions of the ring. The results of associating the measurements in Tables I and II are presented in Table III. The estimation of standard deviation is based on 2000 repetitions of association in one position shows a very small dispersion from the average value, presenting the repeatability of the advanced sonar system.

TABLE 3. TARGET ASSOCIATION RESULTS

	Associated Targets			
	Wall 1	***Corner1***	***Wall 2***	***Corner2***
Pair No	16	19	22	23
Range to Rx (m)	0.5919	0.9974	0.6407	0.6867
Bearing to Rx (deg)	1.9377	0.9851	1.9181	3.5734
STD of Range(m) in 2000 Repetitions	9.13 E-6	1.05 E-5	5.72 E-5	2.76 E-4
STD of Bearing(deg) in 2000 Repetitions	0.0097	0.0103	0.0240	0.2861

5.4. Interference Rejection Concept and Results

In a simultaneously fired sonar ring, multiple transducers must share the same airspace and the pulses transmitted by one transducer may be received by others – this form of interference is also known as crosstalk [16].

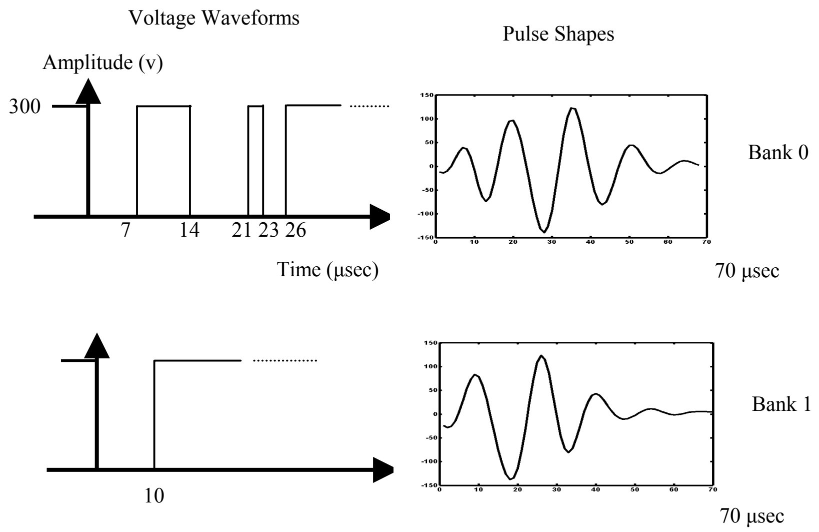

Figure 20. Voltage Waveforms Used to drive the Transmitters and Echo Pulse Shapes of Bank 0 and Bank 1

When the same sonar pulses are used for all transmitters, a receiver cannot determine whether echoes originate from the same pair or from some other pairs of transducers. The matched filtering of all received pulses possibly results in many phantom objects.

In the advanced sonar ring, each slave board can generate its own pulse shape and therefore using different pulse shapes can potentially eliminate most crosstalk. In this experiment, we divided the transducers into two banks, slaves 0, 2 and 4 as bank 0 and slaves 1, 3 and 5 as bank 1. The two banks are interleaved so adjacent pairs of transducers belong to different banks. Fig. 20 shows voltage waveforms and captured echo pulse shapes of bank 0 and bank1.

An experimental comparison that shows the advantages of creating different pulse shapes for adjacent transmitters can be seen in Fig. 21. The phantom objects resulting from crosstalk between two banks are eliminated due to significantly lower correlation than genuine echoes. In this method, different templates for each bank have been saved in DSP, resulting in rejection of more than 50% of crosstalk. In addition, it is possible to have more banks i.e. more pulse shapes to achieve better interference rejection but since interference mostly occurs between adjacent pairs, most of the crosstalk is eliminated with just two banks.

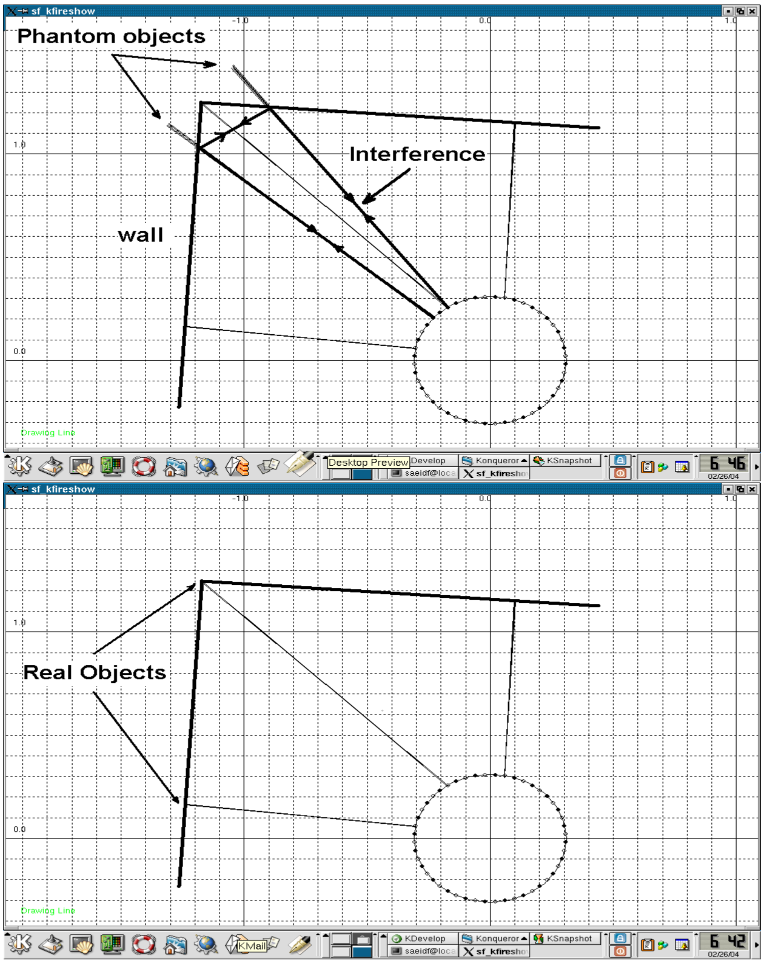

Figure 21. Target Association Results Before and After Applying Interference Rejection Idea

6. Conclusions and Future Work

The report has presented a new approach to a multi DSP real time sonar-ring sensor based on the real time DSP sonar echo processor [8] and the template matched arrival time estimator that has proven accuracy and robustness characteristics [11]. The performance of the sensor has been illustrated by experimental results.

The new sensor has some advantages. Firstly, processing can be done locally obviating the data communication problem to a central computer. Secondly, due to real time signal processing, central processing can be devoted to higher level applications such as simultaneously localization and mapping (SLAM). Finally, the sonar ring enables simultaneous sonar sensing of the surroundings of a robot that is useful for on-the-fly applications on moving platforms.

Future work will be performed on high level applications such as SLAM, obstacle detection and path-planning in real time.

Acknowledgements

We gratefully acknowledge Mr. Steven Armstrong for his assistance in the design and construction of the hardware and basic communication infrastructure of the sonar ring and funding from the ARC Centre for Perceptive and Intelligent Machines in Complex Environments.

References

[1] H. Akbarally, L. Kleeman, Sonar sensor for accurate 3D target localisation and classification, in: Proceedings of the 1995 IEEE International Conference on Robotics and Automation. Part 3 (of 3), May 21-27 1995, Vol. 3 (IEEE, Piscataway, NJ, USA, Nagoya, Jpn, 1995) 3003-3008.

[2] ANALOG-DEVICES, ADSP-2100 FAMILY USER'S MANUAL (Analog Devices, Inc, 1995).

[3] J. Borenstein, Y. Koren, Error eliminating rapid ultrasonic firing for mobile robot obstacle avoidance, IEEE Transactions on Robotics and Automation 11 (1995) 132-138.

[4] J. Budenske, M. Gini, Why is it so difficult for a robot to pass through a doorway using ultrasonic sensors?, in: Proceedings of the 1994 IEEE International Conference on Robotics and Automation, May 8-13 1994 (Publ by IEEE, Piscataway, NJ, USA, San Diego, CA, USA, 1994) 3124-3129.

[5] K.S. Chong, L. Kleeman, Feature-based mapping in real, large scale environments using an ultrasonic array, International Journal of Robotics Research 18 (1999) 3-19.

[6] S. Fazli, L. Kleeman, A Low Sample Rate Real Time Advanced Sonar Ring, in: submitted to the 2004 Australasian Conference on Robotics and Automation, Dec 6-8 2004 (Canberra, Australia, 2004).

[7] S. Fazli, L. Kleeman, A Real Time Advanced Sonar Ring with Simultaneous Firing, in: Accepted for publication at the 2004 IEEE/RSJ International Conference on Intelligent Robotics and Systems, Sep 28-Oct 2 2004 (Sendai, Japan, 2004).

[8] A. Heale, L. Kleeman, A real time DSP sonar echo processor, in: 2000 IEEE/RSJ International Conference on Intelligent Robots and Systems, Oct 31-Nov 5 2000, Vol. 2 (Institute of Electrical and Electronics Engineers Inc., Takamatsu, 2000) 1261-1266.

[9] K.-W. Joerg, M. Berg, Mobile robot sonar sensing with pseudo-random codes, in: Proceedings of the 1998 IEEE International Conference on Robotics and Automation. Part 4 (of 4), May 16-20 1998, Vol. 4 (IEEE, Piscataway, NJ, USA, Leuven, Belgium, 1998) 2807-2812.

[10] L. Kleeman, Fast and accurate sonar trackers using double pulse coding, in: 1999 IEEE/RSJ International Conference on Intelligent Robots and Systems (IROS'99): Human and Environment Friendly Robots whith High Intelligence and Emotional Quotients', Oct 17-Oct 21 1999, Vol. 2 (IEEE, Piscataway, NJ, USA, Kyongju, South Korea, 1999) 1185-1190.

[11] L. Kleeman, R. Kuc, Mobile robot sonar for target localization and classification, International Journal of Robotics Research 14 (1995) 295-318.

[12] L. Kleeman, R. Kuc, Optimal sonar array for target localization and classification, in: Proceedings of the 1994 IEEE International Conference on Robotics and Automation, May 8-13 1994 (Publ by IEEE, Piscataway, NJ, USA, San Diego, CA, USA, 1994) 3130-3135.

[13] P.M.Woodward, Probability and Information Theory with Application to Radar (Oxford:Pergamon Press, 1964).

[14] H. Peremans, K. Audenaert, J.M. Van Campenhout, High-resolution sensor based on tri-aural perception, IEEE Transactions on Robotics and Automation 9 (1993) 36-48.

[15] T. Tsubouchi, Nowadays trends in map generation for mobile robots, in: Proceedings of the 1996 IEEE/RSJ International Conference on Intelligent Robots and Systems, IROS. Part 2 (of 3), Nov 4-8 1996, Vol. 2 (IEEE, Piscataway, NJ, USA, Osaka, Jpn, 1996) 828-833.

[16] M.K. Vlastimil MASEK, Aiguo MING and Ljubisa VLACIC, Fast Mobile Robot Obstacle Detection Using Simultaneous Firing of Sonar Ring Sensors, (1998).

[17] M.K. Vlastimil MASEK, Aiguo MING and Ljubisa VLACIC, A New Method to Improve Obstacle Detection Accuracy Using Simultaneous Firing of Sonar Ring Sensors, The Japan Society for Precision Engineering 33 (1999) 49-54.

[18] P.M. Woodward, probability and Information theory with applications to radar (Pergamon Press, Oxford, 1964).

[19] T. Yata, L. Kleeman, S.i. Yuta, Fast-bearing measurement with a single ultrasonic transducer, International Journal of Robotics Research 17 (1998) 1202-1213.

[20] T. Yata, A. Ohya, S.i. Yuta, Fast and accurate sonar-ring sensor for a mobile robot, Proceedings - IEEE International Conference on Robotics and Automation
Proceedings of the 1999 IEEE International Conference on Robotics and Automation, ICRA99, May 10-May 15 1999 1 (1999) 630-636.

[21] T. Yata, A. Ohya, S.i. Yuta, Using one bit wave memory for mobile robots' new sonar-ring sensors, in: 2000 IEEE International Conference on Systems, Man and Cybernetics, Oct 8-Oct 11 2000, Vol. 5 (Institute of Electrical and Electronics Engineers Inc., Piscataway, NJ, USA, Nashville, TN, USA, 2000) 3562-3567.